Available online at www.sciencedirect.com
ScienceDirect
Journal of the Mechanics and Physics of Solids
55 (2007) 1823–1852

JOURNAL OF THE MECHANICS AND PHYSICS OF SOLIDS

www.elsevier.com/locate/jmps

A novel atomistic approach to determine strain-gradient elasticity constants: Tabulation and comparison for various metals, semiconductors, silica, polymers and the (Ir) relevance for nanotechnologies

R. Maranganti[a], P. Sharma[a,b,*]

[a]*Department of Mechanical Engineering, University of Houston, Houston, TX 77204, USA*
[b]*Department of Physics, University of Houston, Houston, TX 77204, USA*

Received 22 December 2006; accepted 26 February 2007

Abstract

Strain-gradient elasticity is widely used as a suitable alternative to size-independent classical continuum elasticity to, at least partially, capture elastic size effects at the nanoscale. In this work, borrowing methods from statistical mechanics, we present mathematical derivations that relate the strain-gradient material constants to atomic displacement correlations in a molecular dynamics computational ensemble. Using the developed relations and numerical atomistic calculations, the strain-gradient constants are explicitly determined for some representative semiconductor, metallic, amorphous and polymeric materials. This method has the distinct advantage that amorphous materials can be tackled in a straightforward manner. For crystalline materials we also employ and compare results from both empirical and *ab initio* based lattice dynamics. Apart from carrying out a systematic tabulation of the relevant material parameters for various materials, we also discuss certain subtleties of strain-gradient elasticity, including: the paradox associated with the sign of the strain-gradient constants, physical reasons for low or high characteristic length scales associated with

*Corresponding author. Department of Mechanical Engineering, University of Houston, Houston, TX 77204, USA. Tel.: +1 713 743 4256.
E-mail address: psharma@uh.edu (P. Sharma).

0022-5096/$ - see front matter © 2007 Elsevier Ltd. All rights reserved.
doi:10.1016/j.jmps.2007.02.011

the strain-gradient constants, and finally the relevance (or the lack thereof) of strain-gradient elasticity for nanotechnologies.
© 2007 Elsevier Ltd. All rights reserved.

Keywords: Strain gradient elasticity; Nonlocal elasticity; Sign paradox; Atomistic method; Phonon dispersion

1. Introduction

Based upon a set of well-defined axioms, *classical* rational continuum mechanics is explicitly designed to be size-independent (Truesdell and Noll, 1992)—a fact that is well evident in boundary value problems ranging from strain state of a nanoscale quantum dot to effective elastic properties of composites. Novel effects like size-dependency and scaling of mechanical phenomena, which have attracted considerable attention in recent times under various contexts e.g. thin films, quantum dots, plasticity, nanowires, nanotubes and composites amongst others, *cannot* be readily explained by classical continuum mechanics. Thus, there is an expectation that classical elasticity may cease to be valid at nanometer length scales. Several physical reasons may be ascribed to the projected breakdown of continuum elasticity:

(i) *Increasing importance of surface energy*: At the nanoscale, the appreciable surface to volume ratio necessitates accounting for surface/interfacial energies and/or surface elastic effects. Within a field theoretic framework, remedies exist to accommodate these effects e.g. Gurtin and Murdoch (1975, 1978), Cammarata and Sieradzki (1994), Li and Dunn (1998), Steigmann and Ogden (1999), Miller and Shenoy (2000), Kukta et al. (2002), Sharma et al. (2003), Sharma and Ganti (2004), Duan et al. (2005), He et al. (2004) and Mi and Kouris (2006).

(ii) *Discrete nature of matter*: The assumption of a smeared-out elastic continuum, central to classical continuum mechanics, is no longer valid at the nanoscale where the discrete atomistic nature of matter becomes apparent. Classical continuum elasticity fails to adequately capture several phenomena at the level of a few lattice spacings. Further, the fluctuations in the interatomic forces and their long-range character may induce non-local behavior that is in contradiction to the postulated local character of classical elasticity. Researchers often see enriched continuum theories like non-local elasticity as a means to approximately model the true non-local behavior of the material. Pioneering work in this direction can be traced to Toupin (1962), Koiter (1964), Mindlin (1964, 1965) and Krumhansl and Kroner (1968). Some other representative contributions are: Eringen and Edelen (1972), Kunin (1982, 1984), Kleinert (1989); Reid and Gooding (1992), Ru and Aifantis (1993), Aifantis (1999), Lam et al. (2003), Zhang and Sharma (2005a, b), and Park and Gao (2006).

(iii) *Presence of defects and microstructure*: The correlations of the elastic fields of defects such as dislocations and inhomogeneities may lead to a coarse-grained elastic response that is size-dependent and non-local in character. For further discussion in this context the reader is referred to Kroner (1970), Gutkin and Aifantis (1999), Gutkin (2000), Forest et al. (2000), Drugan (2000), Frantziskonis and Aifantis (2002), Bouyge et al. (2001), Fatemi et al. (2002), Groma et al. (2003) and Onck (2003).

(iv) *Internal strain*: For certain types of materials, increasing prominence of internal motions within a non-primitive lattice result in additional degrees of freedom above and

beyond the classical displacement degrees of freedom which cannot be accounted for by classical elasticity theory (say, for example, in liquid crystals, polymers and granular materials). In such cases, if a field theory is desired, recourse must be made to the so-called director field theories such as the micromorphic theory or its more popular subsets: the Cosserat theory and micropolar elasticity. For additional details, the interested reader is referred to a review by Eringen (1999) and other works due to Green and Rivlin (1964), Cheng and He (1995, 1997), Sharma and Dasgupta (2002) and Chen et al. (2003, 2004).

(v) *Quantum confinement*: It has been recently shown (in the context of semiconductor quantum dots) that quantum confinement may induce a strain field even in complete absence of an external stress. Such an effect, which scales with the square of the wave-function, is inversely proportional to the volume of the nanostructure (Zhang et al., 2007) and is of importance only in the size-range below 2 nm.

An obvious route to investigate elastic phenomena at nanometric length scales incorporating the physical effects (i)–(v) listed above would be via discrete atomistic simulations. However, field theoretic methods in the same vein of classical continuum elasticity, albeit ones that capture the aforementioned size effects (if any), are desirable as well since they are often computationally more tractable, and for simpler problems, lead to physically illuminating analytical solutions. Strain-gradient elasticity, which is one type of a non-local theory of elasticity, is often invoked to phenomenologically capture the size effects within the purview of the physical effects noted in (ii) and (iii). Although extensive literature has now appeared on non-local elasticity theories, relatively little work[1] (DiVincenzo, 1986; Opie and Grindlay, 1972; Shibutani et al., 1998; Hao and Maris, 2000, 2001; Lam et al., 2003; McFarland and Colton, 2005) has gone into ascertaining the material parameters that dictate the "strength" of the aforementioned non-local effects. The magnitude of the strain-gradient constants has an important bearing on whether there exists a need for strain-gradient elasticity or whether classical continuum elasticity is a sufficiently good approximation while investigating nanoscale elastic phenomena.

In this work, we:

(i) introduce a novel molecular dynamics (MD) based method to determine strain-gradient constants. Borrowing methods from statistical mechanics, we derive equations that relate the dynamic strain-gradient material constants to the displacement correlations in a MD computational ensemble.
(ii) tabulate the strain-gradient elasticity parameters for various representative material systems such as metals (Cu, Al), single (Si, Ge, C) and multi-component semiconductors (GaAs, GaP), amorphous silica and a polymeric system (polythene).
(iii) discuss certain subtleties of strain-gradient elasticity including: the paradox associated with the sign of the dynamic strain-gradient constants, technicalities associated with atomistic calculations of the aforementioned material parameters, the physical reasons for low or high length scales associated with the dynamic strain-gradient constants, the special case of non-centrosymmetric crystals and finally the relevance (or the lack thereof) of strain-gradient elasticity for nanotechnologies.

The outline of our paper is as follows. Section 2 consists of a brief introduction to strain-gradient elasticity followed by a discussion on the strain-gradient material constants. In

[1]Also see Chen et al. (2003, 2004) for work more focused on micromorphic theories.

Section 3, we describe how the phenomenological strain-gradient elasticity theory can be linked to microscopic lattice dynamics; in particular we discuss how both empirical and *ab initio* lattice dynamics may be employed to extract strain-gradient elasticity constants. In Section 4, we present a new MD based technique to determine the strain-gradient elasticity constants by means of calculating the atomic displacement correlations in an NVT (constant number of particles N, constant volume V and constant temperature T) ensemble. In Section 5, we discuss (and try to resolve) apparent inconsistencies in the sign of the strain-gradient constants which arise when strain-gradient theory is required to be thermodynamically stable while simultaneously exhibiting physically acceptable phonon dispersion characteristics. The numerical values of the strain-gradient constants are presented in Section 6 for various representative materials while, in light of the numerical results, Section 7 includes a general discussion on the relevance of strain-gradient elasticity nanotechnologies. Also, in Section 7, we try to argue the physical reasons that may be responsible for the observed magnitudes of the strain-gradient constants of the investigated material systems.

2. Governing equations of strain-gradient elasticity and material constants

Within the assumption of a linearized theory of a homogeneous elastic medium incorporating terms involving first and second gradients of the displacement gradient, one can write a phenomenological expression for the Lagrangian density "L" for a solid (Mindlin, 1964; DiVincenzo, 1986) in the following manner:

$$L = \tfrac{1}{2}\rho \dot{u}_i \dot{u}_i - \tfrac{1}{2} C_{ijkl} e_{ij} e_{kl} - D_{ijklm} u_{i,j} u_{k,lm} - F^1_{ijklmn} u_{i,jk} u_{l,mn} - F^2_{ijklmn} e_{ij} u_{k,lmn} - \cdots . \quad (1)$$

Here, ρ is the mass density of the solid, $\mathbf{u}$ is the displacement field; the dot on top of u_i denotes differentiation with respect to time and the comma denotes differentiation with respect to the spatial variables in the reference configuration. $\mathbf{e}$ is the symmetric strain tensor defined as

$$\mathbf{e} = \tfrac{1}{2}(\nabla \mathbf{u} + \nabla \mathbf{u}^{\mathrm{T}}). \quad (2)$$

Both indical and direct notations will be used as convenient. The first term on the right-hand side of Eq. (1) is the kinetic energy and the remaining terms constitute the potential energy. The potential energy density of Eq. (1) is invariant under the Euclidean group $\mathrm{SO}(3) \triangleright \mathrm{T}(3)$ i.e. the semi-direct product of the rigid rotation group SO(3) and the rigid translation group T(3). Invariance under rigid translations ensures that the internal energy density can only depend upon the first- and higher-order derivatives of the displacement, $\nabla \otimes \nabla \otimes \cdots \otimes \mathbf{u}$ and not on the displacement $\mathbf{u}$ itself. Invariance restrictions under rigid rotations only permit the symmetric part of the displacement gradient i.e. the strain defined by Eq. (2) to contribute to the internal energy density expression. However, starting from the second derivative, all higher derivatives of the displacement vector i.e. $\nabla \otimes \nabla \otimes \cdots\cdots \otimes \mathbf{u}$ transform properly under $\mathrm{SO}(3) \triangleright \mathrm{T}(3)$. The first term in the expression for potential energy $\frac{1}{2} C_{ijkl} \varepsilon_{ij} \varepsilon_{kl}$ in Eq. (1) describes the long-wavelength elastic excitations of the solid—the lowest-order description of sound. The coefficients C_{ijkl} are the conventional elastic constants of the solid. At larger length scales (assuming small deformations and rotations), the term involving C_{ijkl} dominates the potential energy and the higher-order gradient terms involving the coefficients $\mathbf{D}$, $\mathbf{F}^1$ and $\mathbf{F}^2$ provide negligible contributions.

However, in the presence of large strain gradients the contributions due to these higher-order terms may prove to be significant and is in fact the *raison d' etre* for this theory.

To derive the equation of motion from the Lagrangian in Eq. (1) we rewrite it as

$$L = \tfrac{1}{2}\rho\dot{u}_i\dot{u}_i - \tfrac{1}{2}C_{ijkl}u_{i,j}u_{k,l} - D_{ijklm}u_{i,j}u_{k,lm} - F^1_{ijklmn}u_{i,jk}u_{l,mn} - F^2_{ijklmn}u_{i,j}u_{k,lmn} - \cdots. \tag{3}$$

The symmetry of the strain tensor with respect to its two indices is reflected in the material constant tensors $\mathbf{C}$ and $\mathbf{F}^2$ in Eq. (3) which are symmetric with respect to the indices i and j. The subsequent variational analysis follows exactly from DiVincenzo (1986). For the variations in the action "A" to be stationary we must have,

$$\delta A = \delta\left[\int L\,\mathrm{d}x\,\mathrm{d}t\right] = 0, \tag{4a}$$

$$\delta A = \int \mathrm{d}x \int \mathrm{d}t \left\{ \begin{array}{c} \rho\delta\dot{u}_\alpha\dot{u}_\alpha - \tfrac{1}{2}C_{ijkl}[(\delta u_i)_{,j}u_{k,l} + (\delta u_k)_{,l}u_{i,j}] \\ -D_{ijklm}[(\delta u_i)_{,j}u_{k,lm} + (\delta u_k)_{,lm}u_{i,j}] \\ -F^1_{ijklmn}[(\delta u_i)_{,j}u_{k,lmn} + (\delta u_k)_{,lmn}u_{i,j}] \\ -F^2_{ijklmn}[(\delta u_i)_{,jl}u_{k,mn} + (\delta u_k)_{,mn}u_{i,jl}] \end{array} \right\}. \tag{4b}$$

Now integrating Eq. (4b) by parts one obtains the elastic equations of motion as

$$\rho\ddot{u}_i = c_{ijkl}u_{k,lj} + d_{ijklm}u_{k,lmj} + f_{ijklmn}u_{k,lmnj}. \tag{5}$$

The material constants $\mathbf{c}$, $\mathbf{d}$ and $\mathbf{f}$ are referred to as the "dynamic elastic constants" and can be expressed in terms of the static elastic constants $\mathbf{C}$, $\mathbf{D}$, $\mathbf{F}^1$ and $\mathbf{F}^2$ as

$$c_{ijkl} = \mathrm{sym}_{(i,k)}\mathrm{sym}_{(j,l)}C_{ijkl}, \tag{6a}$$

$$d_{ijklm} = \mathrm{asym}_{(i,k)}\mathrm{sym}_{(j,l,m)}D_{ijklm}, \tag{6b}$$

$$f_{ijklmn} = \mathrm{sym}_{(i,k)}\mathrm{sym}_{(j,l,m,n)}(F^2_{ijklmn} - F^1_{ijlkmn}). \tag{6c}$$

The symbols "sym" and "asym", respectively, denote symmetrization and anti-symmetrization with respect to the indices in the subscripts. While the symmetrization (antisymmetrization) with respect to indices i and k follows from the integration by parts referred to above, the symmetrization with respect to the remaining indices is borne out by commutation property of the derivative operation. While Eq. (6a) can be completely inverted (Lax, 1974) (i.e. it is possible to uniquely recover the entire classical elastic constant tensor C_{ijkl} from the dynamic elastic constant tensor c_{ijkl}), Eqs. (6b) and (6c) are non-invertible i.e. one cannot completely recover the static elastic constants $\mathbf{D}$, $\mathbf{F}^1$ and $\mathbf{F}^2$ from the dynamic elastic constants $\mathbf{d}$ and $\mathbf{f}$, respectively.

It is of interest to note that the fifth-order tensor $\mathbf{d}$ in Eq. (5) has attracted some attention in the literature as it describes a phenomenon observed in some solids called "acoustic activity" (Mindlin, 1964; Portigal and Burnstein, 1968; Every, 2005). This so-called acoustic activity is analogous to the well-known phenomenon of optical activity which describes the effect of spatial dispersion on the propagation of electromagnetic light waves. Optical activity can be attributed to first-order dispersive contributions to the dielectric constant tensor which typically, is a function of the frequency alone and does not depend upon the wave-vector. This dispersive effect in turn can be explained by invoking a

non-local dependence of the electric displacement vector **D** on the electric field vector **E**. The spatial-dispersive contributions to the dielectric constant $\boldsymbol{\varepsilon}$ can be included in a phenomenological fashion by expanding $\boldsymbol{\varepsilon}$ as a power series in the wave-vector **k** as follows:

$$\varepsilon_{ij}(\omega,\mathbf{k}) = \varepsilon_{ij}(\omega) + ig_{ijl}(\omega)k_l + h_{ijlm}(\omega)k_lk_m + \cdots. \tag{7}$$

Optical activity is a consequence of the term $ig_{ijl}(\omega)k_l$, and the tensor **g** is referred to as the gyrotropic tensor. The dynamic elastic tensor **d** in our description is analogous to the gyroscopic tensor **g** in that it provides a first-order wave-vector dependence to the dynamic elastic constant tensor **c** (DiVincenzo, 1986).

If one assumes a plane-wave solution of the form $u_i = u_i^0 \exp \mathrm{i}(\omega t + \mathbf{k}\cdot\mathbf{r})$ for Eq. (5)[2] then

$$\rho\omega^2 u_i^0 = (c_{ijkl}k_jk_l + id_{ijklm}k_jk_lk_m - f_{ijklmn}k_jk_lk_mk_n)u_k^0. \tag{8}$$

Eq. (8) can be re-written in the following form:

$$\rho\omega^2 u_i^0 = R_{ik}(\mathbf{k})u_k^0. \tag{9}$$

$R(\mathbf{k})$ is the *dynamical matrix* derived in a purely elastic continuum framework. The eigenvalue problem posed by Eq. (8) can be solved to express the frequency ω in terms of the wave-vector **k** which leads to the *phonon dispersion relations*. Eq. (9) provides three such dispersion relations which represent the acoustic phonon modes or sound waves traveling through the solid.

The classical elastic limit of Eq. (8) can be obtained by setting the coefficients of tensors **d** and **f** to zero to obtain

$$\rho\omega^2 u_i^0 = (c_{ijkl}k_jk_l)u_k^0, \tag{10}$$

which leads to a linear ω vs. **k** relationship. While this relationship certainly holds true for almost all materials at values of the **k** in the vicinity of zero, dispersive effects start to kick in at higher **k**-vectors wherein the phonon dispersion relations start deviating from the linear relationship reflected by Eq. (10). In particular, for most crystals when the phonon frequencies are of the order of 1 THz, the ω vs. **k** phonon curves start dipping downwards (see Fig. 1), an effect that obviously cannot be accounted for by the classical continuum elasticity model in Eq. (10). On the other hand, the phonon dispersion relations of Eq. (8) obtained from the extended strain-gradient elasticity theory can capture these non-linear effects at high **k**-vectors provided that the signs of the components of the dynamic strain-gradient constants **d** and **f** are such that they model the correct dispersive behavior of phonons.

A group theoretical analysis to determine the number of independent components of tensors **c**, **d** and **f** for crystals possessing point-group symmetry $43m$ (corresponding to a cubic Zinc-blende type crystal like GaAs) has already been carried out by DiVincenzo (1986). The classical dynamical elastic constant **c** has three independent components c_{1111}, c_{1212} and c_{1122}; the fifth-order tensor **d** has only one independent component d_{12223} while the sixth-order tensor **f** happens to have six independent components f_{111111}, f_{122122}, f_{112222}, f_{122133}, f_{112233} and f_{211222}. The remaining elements of these tensors can be generated

[2]This can be done since a perfect crystal is transitionally invariant.

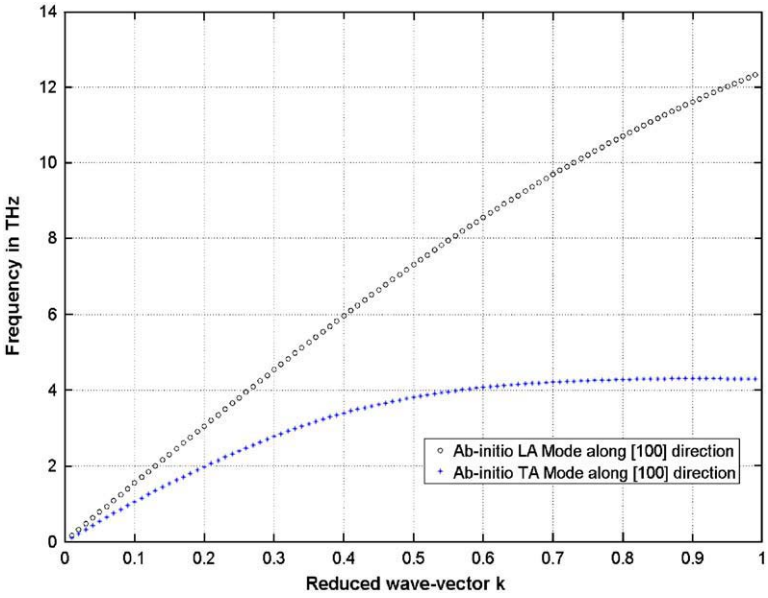

Fig. 1. The longitudinal acoustic (LA) and transverse acoustic (TA) phonon dispersion curves of Silicon along [1 0 0] direction generated by *ab initio* calculations are shown.

by suitable permutations of the tensor indices. It should be noted that for centrosymmetric diamond-like crystals like Si or fcc type crystals like Cu, the odd-order tensor **d** vanishes.

From Eqs. (8) and (9), the dynamical matrix $R(\mathbf{k})$ can now be written in terms of the independent components of tensors **c**, **d** and **f**.

$$R_{ii} = c_{1111}k_i^2 + c_{1212}(k_j^2 + k_k^2) - f_{111111}k_i^4 - f_{122122}(k_j^4 + k_k^4) - 6f_{122133}k_j^2k_k^2 - 6f_{211222}(k_i^2k_j^2 + k_i^2k_k^2), \tag{11a}$$

$$R_{ij} = 2c_{1122}k_ik_j + 3id_{12223}(k_i^2k_k - k_j^2k_k) - 4f_{112222}(k_ik_j^3 + k_i^3k_j) - 12f_{112233}(k_ik_jk_k^2). \tag{11b}$$

It should be noted that since the matrix $id_{ijklm}k_kk_lk_m$ has zero-diagonal elements, it will only contribute to the phonon dispersions in second-order perturbation theory. A typical contribution is of the form $|d_{ijklm}k_jk_lk_m|^2/\rho(\omega_i^2 - \omega_k^2)k^2$ whose order k^4 is of the same order as the contribution due to **f**. This perturbative result is not expected to hold along the high-symmetry axes [1 0 0] and [1 1 1] since the eigenvalues of the dynamical matrix are degenerate along these axes. However, as it turns out for cubic crystals of the GaAs type, the numerator $|d_{ijklm}k_jk_lk_m|^2$ also vanishes so the above conclusion regarding the contribution of the **d** tensor to the phonon dispersions still holds.

3. Linking strain-gradient elasticity to lattice dynamics: empirical and *ab initio*

In contrast with the continuum approach, from the microscopic lattice-dynamical viewpoint, the dynamical matrix $R(\mathbf{k})$ for a crystalline solid with more than one atom in its

unit cell is defined by (Maradudin et al., 1971)

$$R_{ik}^{\alpha\beta}(\mathbf{k}) = \frac{\rho}{\sqrt{M_\alpha M_\beta}} \sum_p K_{ik}^{\alpha p \beta q} \exp[\mathrm{i}\mathbf{k}.(\mathbf{X}^{\beta q} - \mathbf{X}^{\alpha p})]. \tag{12}$$

Here ρ is the density of the material; M_α and M_β are the masses of the αth and the βth atoms, respectively. $K_{ik}^{\alpha p \beta q}$ is the so-called *atomic force constant matrix*. To a first approximation the coefficient $K_{ik}^{\alpha p \beta q}$ can be regarded as the negative of the force exerted in the ith direction on the αth atom in the pth unit cell, when the βth atom situated in the qth unit cell is displaced in the jth direction by a unit distance, all the other atoms being kept at their equilibrium position.

Analogous to Eq. (9), the equations of motion can be written as

$$\rho\omega^2(\mathbf{k}) u_i^\alpha(\mathbf{k}) = R_{ik}^{\alpha\beta}(\mathbf{k}) u_k^\beta(\mathbf{k}). \tag{13}$$

Now let us examine the link between the phenomenological strain-gradient elasticity theory and the microscopic lattice-dynamical approach. In a discrete lattice-dynamical setting, the dynamical matrix (Eq. (12)) for a simple Bravais-lattice (1 atom per unit cell) becomes

$$R_{ik}(\mathbf{k}) = \frac{1}{\Omega_0} \sum_n K_{ik}^{mn} \exp[\mathrm{i}\mathbf{k}.(\mathbf{X}^n - \mathbf{X}^m)]. \tag{14}$$

Here, Ω_0 is the volume of the unit cell.

The corresponding equations of motion become

$$\rho\omega^2(\mathbf{k}) u_i^0(\mathbf{k}) = R_{ik}(\mathbf{k}) u_k^0(\mathbf{k}). \tag{15}$$

The long-wavelength limit ($\mathbf{k} \to 0$) of Eq. (15) can be obtained by expanding $R(\mathbf{k})$ in powers of $\mathbf{k}$ until the first non-vanishing term to obtain

$$\rho\omega^2 u_i^0 = c'_{ijkl} k_j k_l u_k^0. \tag{16}$$

The constants c'_{ijkl} are given as (Lax, 1974, p. 347)

$$c'_{ijkl} = -\frac{1}{2\Omega_0} \sum_n K_{ik}^{mn} (\mathbf{X}^n - \mathbf{X}^m)_a (\mathbf{X}^n - \mathbf{X}^m)_b. \tag{17}$$

The constants c'_{ijkl} possess the same symmetry as the dynamic elastic constants c_{ijkl} of Eq. (8) and therefore correspond to a similar tensor. This is the reason why classical continuum elasticity theory is sometimes referred to as a *long-wavelength approximation* of lattice-dynamical theory. Similarly, one can carry out the expansion of Eq. (15) into higher powers of $\mathbf{k}$ and identify microscopic material constants which resemble the dynamic elastic constants $\mathbf{d}$ and $\mathbf{f}$ of Eq. (8). Indeed, simple expressions for the strain-gradient elasticity constants have been derived for fcc cubic crystals interacting via a Lennard-Jones potential by Opie and Grindlay (1972).

However, the identification between the discrete and continuum approaches is not so readily apparent when the crystal lattice ceases to be a Bravais lattice. Eq. (8) derived from a purely continuum framework consists of three equations of motion. On the other hand, Eq. (12) derived from a lattice-dynamical point of view consists of $3N$ equations of motion, N being the number of atoms per unit cell. Three solutions to this eigenvalue problem posed by Eq. (13) correspond to acoustic phonons while the remaining $3(N-1)$ modes are the optical phonon modes. For the case of a simple Bravais lattice (like fcc metals Cu and

Al) where $N = 1$, Eq. (13) (which reduces to Eq. (15)) too yields three equations of motion which correspond to acoustic phonon modes (optical modes are absent) and the dynamic elastic constants of Eq. (7) can be trivially read off from a power series expansion of the dynamical matrix of Eq. (15) in terms of $\mathbf{k}$. However, as DiVincenzo (1986) points out, for $N > 1$, the identification is not so straightforward since the acoustic and optical contributions are coupled to each other in the dynamical matrix. DiVincenzo (1986) has outlined an analytic procedure based on Lax (1974) to isolate the acoustic and optical contributions to the dynamical matrix at any $\mathbf{k}$-vector for cubic crystals with unit cells containing two atoms ($N = 2$). This class of crystal includes single-component semiconductors/insulators like Si, Ge, diamond etc., III–V semiconductors like GaAs, GaP, InAs, etc. and II–VI semiconductors/insulators like CdSe, ZnS, ZnO, etc. We briefly discuss DiVincenzo's procedure in the following paragraphs.

At $\mathbf{k} = (0, 0, 0)$ (the Gamma-point), the 6×6 dynamical matrix $R(\mathbf{k})$ can be block-diagonalized by applying a unitary transformation U (which consists of the $\mathbf{k} = 0$ eigenvectors). The transformed matrix R^U now is a diagonal matrix consisting of the eigenvalues of $R(\mathbf{k})$

$$R^U(\mathbf{k} = 0) = U^{\mathrm{T}} R(\mathbf{k} = 0) U = \begin{bmatrix} D^{\mathrm{a}}_{3\times3} & 0_{3\times3} \\ 0_{3\times3} & D^{\mathrm{o}}_{3\times3}. \end{bmatrix}. \tag{18}$$

Matrices D^{a} and D^{o} are the acoustic and optic contributions to the dynamical matrix, respectively. The 3×3 matrix D^{a} is identified with the dynamical matrix obtained from classical continuum elasticity in Eq. (8). For $\mathbf{k} \neq 0$, if the same unitary transformation is applied to the dynamical matrix then the resulting transformed matrix is not completely uncoupled and the acousto-optical couplings remain of a small order in $\mathbf{k}$,

$$R^U(\mathbf{k}) = U^{\mathrm{T}} R(\mathbf{k}) U = \begin{bmatrix} D^{\mathrm{a}}_{3\times3} + \mathrm{O}(\mathbf{k}) I_{3\times3} & \mathrm{O}(\mathbf{k}) I_{3\times3} \\ \mathrm{O}(\mathbf{k}) I_{3\times3} & D^{\mathrm{o}}_{3\times3} + \mathrm{O}(\mathbf{k}) I_{3\times3} \end{bmatrix}. \tag{19}$$

It should be pointed out that the above statement assumes that the dynamical matrix that results out of the lattice-dynamical model being employed is analytic in the vicinity of $\mathbf{k} = 0$. This is not the case for polar crystals where the Coulombic contributions to the dynamical matrix have a macroscopic field term of the form $k_\alpha k_\beta / k^2$. However, for non-polar and slightly polar crystals the effect of the non-analyticity may be taken to be small and the expression in Eq. (19) is correct. Thus, one should be able to find an additional small orthogonal transformation of the form $\exp(\mathrm{i}\delta H)$ (where δH is a small Hermitian matrix) which completely decouples the acoustic and optical subspaces as follows:

$$\exp(-\mathrm{i}\delta H) R^U(\mathbf{k}) \exp(\mathrm{i}\delta H) = \begin{bmatrix} D^{\mathrm{a}}_{3\times3} & 0_{3\times3} \\ 0_{3\times3} & D^{\mathrm{o}}_{3\times3} \end{bmatrix}. \tag{20}$$

A perturbative-theoretic approach has been employed by DiVincenzo (1986) to determine δH. The transformed dynamical matrix is divided into three parts: $R^U(\mathbf{k}) = H_0 + Y(\mathbf{k}) + X(\mathbf{k})$.

$$H_0 = R^U(\mathbf{k} = 0) = \begin{bmatrix} E^{\mathrm{a}} I_{3\times3} & 0_{3\times3} \\ 0_{3\times3} & E^{\mathrm{o}} I_{3\times3} \end{bmatrix},$$

$$Y(\mathbf{k}) = \begin{bmatrix} R^U_{\mathrm{aa}}(\mathbf{k}) & 0_{3\times 3} \\ 0_{3\times 3} & R^U_{\mathrm{oo}}(\mathbf{k}) \end{bmatrix} - R^U(\mathbf{k}=0),$$
$$X(\mathbf{k}) = \begin{bmatrix} 0_{3\times 3} & R^U_{\mathrm{ao}}(\mathbf{k}) \\ R^U_{\mathrm{oa}}(\mathbf{k}) & 0_{3\times 3}. \end{bmatrix}. \tag{21}$$

δH can be solved for iteratively by expanding the exponential of Eq. (20) and is found out to be (DiVincenzo, 1986)

$$\delta H = -\mathrm{i}X^H + \mathrm{i}[Y, X^H]^H - \cdots. \tag{22}$$

For a matrix of the form $A = \left[\begin{smallmatrix} 0_{3\times 3} & A^{12}_{3\times 3} \\ A^{21}_{3\times 3} & 0_{3\times 3} \end{smallmatrix}\right]$, A^H is defined as

$$A^H = \begin{bmatrix} 0_{3\times 3} & \frac{A^{12}_{3\times 3}}{E^{\mathrm{a}} - E^{\mathrm{o}}} \\ \frac{A^{21}_{3\times 3}}{E^{\mathrm{o}} - E^{\mathrm{a}}} & 0_{3\times 3} \end{bmatrix}. \tag{23}$$

The acousto-optical coupling terms can be made smaller and smaller by approximating δH better by including additional terms which are represented by the dots in Eq. (22).

The form of δH from Eq. (22) can be substituted in Eq. (20) to obtain an expression for the uncoupled matrix of Eq. (20).

$$\begin{bmatrix} D^{\mathrm{aa}}(\mathbf{k}) & 0_{3\times 3} \\ 0_{3\times 3} & D^{\mathrm{oo}}(\mathbf{k}) \end{bmatrix} = \sum_{j=0}^{\infty} K^{(j)}, \tag{24}$$

where the $K^{(j)}$'s are given by

$$K^{(0)} = H_0, K^{(1)} = Y, K^{(2)} = \frac{1}{2}[X^H, X],$$
$$K^{(3)} = \frac{1}{2}[X, [Y, X^H]^H],$$
$$K^{(4)} = \frac{1}{2}\left[X, \left\{[[Y, X^H]^H, Y]^H + \frac{2}{3}[K^{(2)}, X^H]^H\right\}\right] - \frac{1}{12}[[K^{(2)}, X^H], X^H]. \tag{25}$$

The $K^{(j)}$'s in Eq. (25) correspond to successively higher powers of the wave-vector $\mathbf{k}$, though the correspondence is not one-to-one. The contribution of terms in Eq. (24) starting from $K^{(5)}$ onwards is of the order of k^5 and up. Therefore, we need not consider them for our purpose since the strain-gradient constants $\mathbf{d}$ and $\mathbf{f}$ are associated with a k^3 and a k^4 term, respectively.

Following DiVincenzo's (1986) procedure, one can readily extract the elastic constants from an appropriately chosen lattice-dynamical model. Over the years, several empirical lattice-dynamical models have been developed such as the rigid-ion model, deformable-ion model, polarizable bond charges model, rigid valence shell model, etc. For a detailed description of each model the reader is referred to the following literature: Lax (1974), Maradudin et al. (1971) and Kunc and Nielsen (1979a, b). Using any of these models, we can compute the dynamical matrix $R^U(\mathbf{k})$ for any value of $\mathbf{k}$. Eqs. (24) and (25) can then be used to evaluate the dynamical matrix: these expressions are correct up to order k^4. To extract the elastic constants, we simply fit to the expressions for certain elastic dynamical matrix elements of Eqs. (11a, b) along high-symmetry directions in $\mathbf{k}$. The fitting described above is sufficient to over-determine the dynamic elastic constants and therefore

consistency checks need to be carried out to ensure the accuracy of the determined elastic constants.

For empirical lattice-dynamical models, DiVincenzo's procedure outlined above can be performed analytically. The matrix given by Eq. (24) can be obtained in terms of **k**, and the coefficients of k^4 can be isolated and identified with various dynamical elastic constants according to Eqs. (11). On the other hand, when one employs an *ab initio* approach, it is impossible to calculate the dynamical matrix analytically and hence the coefficients of the k^3 and k^4 (the **d** and the **f** tensors, respectively) in the dynamical matrix cannot be isolated and compared with those of Eqs. (11a, b). However, a numerical fitting procedure of the phonon dispersion relations along high-symmetry directions can be employed to find out the requisite dynamic elastic constants. Given the state of the art of theoretical condensed-matter physics and of computational materials science, phonon dispersions of simple materials are routinely calculated using *ab initio* quantum mechanical techniques which only require the chemical composition of the material in question as input. One of the most popular *ab initio* techniques is the density-functional theory (DFT) (Hohenberg and Kohn, 1964; Kohn and Sham, 1965); a further development is the density-functional perturbation theory (Zein, 1984; Baroni et al., 1987). The phonon dispersions obtained from these techniques compare very well with observed experimental neutron-diffraction data and indeed when experimental data are hard to come by, data generated from *ab initio* techniques are very often used to investigate the properties of materials. Several resources on *ab initio* techniques, their implementation and subsequent applications to materials abound in the literature, most notable of them being Giannozzi et al. (1991), Baroni et al. (2001) and Bamzai and Deb (1981). In this work, we have used the Quantum-ESPRESSO package which implements density-functional perturbation theory (Baroni et al., 2001) to calculate the *ab initio* phonon dispersion relations.

For calculating the phonon dispersion curves over the entire Brillouin zone using codes available in the Quantum-ESPRESSO package, the dynamical matrices are first calculated for a specified grid of **k** vectors e.g. a Chadi-Cohen grid consisting of 10 **k** points or say a $(4 \times 4 \times 4)$ **k**-point grid. With the dynamical matrices over a suitable grid of **k** points in hand, an inverse Fourier transform can be carried out to obtain the real-space force constants (see Eq. (29)). Since typically phonon frequencies are continuous functions of the wave-vector **k**, these force constants can be then used to calculate the phonon frequencies over the entire Brillouin zone. It has to be mentioned that the density of the **k**-vector grid that one starts out with should be chosen according to the material system one is investigating. From the form of the Fourier transform of Eq. (29), it can be seen that the denser the grid of the **k** vectors, the larger the vector **R** for which the inter-atomic force constants are calculated. While for non-polar systems like say Si, the inter-atomic force constants are relatively short range, thereby requiring a moderate number of calculations at different **k** (say 10 **k** points) for computing the phonon dispersions reasonably accurately, polar systems like GaAs possess long-range interactions and therefore a denser **k**-point grid (say one consisting of 60 **k** points) can ensure that the inter-atomic force constants obtained span the range of the inter-atomic interactions and hence accurate phonon spectra are obtained. Material-specific technicalities involved in calculating the *ab initio* phonon dispersions have been mentioned in more detail in Section 6.

We now discuss the extraction of strain-gradient elasticity constants from phonon dispersions generated from *ab initio* calculations. Consider the acoustic 3×3

dynamical matrix (derived from our extended elasticity theory) of Eq. (11) along the high-symmetry direction $\mathbf{k} = (1\,0\,0)$ for a *centrosymmetric* material. Substituting the form of the wave-vector into Eq. (11), the 3×3 dynamical matrix R takes the following form:

$$R|_{3\times 3} = \begin{bmatrix} c_{1111}k^2 + f_{111111}k^4 & 0 & 0 \\ 0 & c_{1212}k^2 + f_{122122}k^4 & 0 \\ 0 & 0 & c_{1212}k^2 + f_{122122}k^4 \end{bmatrix}. \tag{26}$$

Thus, we can see that along the direction $\mathbf{k} = (1\,0\,0)$, the acoustic 3×3 dynamical matrix predicted by continuum elasticity (Eq. (11)) is completely diagonalized. Now, using *ab initio* techniques one can generate the eigenfrequencies of the complete dynamical matrix along the direction $\mathbf{k} = (1\,0\,0)$ for several $\mathbf{k}$ vectors starting from $\mathbf{k} = (0\,0\,0)$ to say $\lambda(1\,0\,0)$. For a crystal containing two atoms per unit cell, this diagonalized matrix will be a 6×6 square matrix of the form

$$\begin{bmatrix} \underline{D}^{\mathrm{aa}}(k)|_{3\times 3} & \underline{0}\,|_{3\times 3} \\ \underline{0}\,|_{3\times 3} & \underline{D}^{\mathrm{oo}}(k)|_{3\times 3} \end{bmatrix}. \tag{27}$$

In the above expression, the acoustic part of the dynamical matrix (generated from *ab initio* calculations) $\underline{D}^{\mathrm{aa}}(k)|_{3\times 3}$ and the optical part of the dynamical matrix $\underline{D}^{\mathrm{oo}}(k)|_{3\times 3}$ are 3×3 diagonal matrices themselves. The acoustic part of the dynamical matrix $\underline{D}^{\mathrm{aa}}(k)|_{3\times 3}$ along $\mathbf{k} = k(1\,0\,0)$ is constrained by lattice-dynamical considerations to assume the form

$$\underline{D}^{\mathrm{aa}}(k)|_{3\times 3} = \begin{bmatrix} l & 0 & 0 \\ 0 & m & 0 \\ 0 & 0 & m \end{bmatrix}. \tag{28}$$

Now, the acoustic-dynamical matrices given by Eq. (26) (from continuum method) and Eq. (28) (from *ab initio* calculations) can be compared with each other at different $\mathbf{k}$ vectors and a numerical fitting can be carried out to determine the components $c_{1111}, f_{111111}, c_{1212}$ and f_{122122}. It must however be realized that the fit should be carried out starting from $\mathbf{k}$-vectors in the vicinity of zero to $\mathbf{k}$ vectors where the dispersive effects just start to kick in since we are only interested to capture the first-order correction to the linear ω vs $\mathbf{k}$ relationship. Fitting at $\mathbf{k}$ vectors which correspond to regions where frequencies are very high and dispersive effects are large will result in spurious estimates for the dynamic elastic constants. In this work, a non-linear least-square minimizing technique has been employed and the components of the $\mathbf{k}$ vectors (k_1, k_2, k_3) which have been employed for the fitting are such that $|k_i| < 0.05$.

Now along, $\mathbf{k} = k(1\,1\,0)$, the 3×3 dynamical matrix predicted by continuum elasticity of Eqs. (11a, b) has the following form:

$$R|_{3\times 3} = \begin{bmatrix} a(k) & b(k) & 0 \\ b(k) & a(k) & 0 \\ 0 & 0 & c(k) \end{bmatrix}. \tag{29}$$

The functions a, b and c are given by

$$a(k) = (c_{1111} + c_{1212})k^2 + (f_{111111} + f_{122122} + 6f_{211222})k^4,$$
$$b(k) = 2c_{1122}k^2 + 8f_{112222}k^4,$$
$$c(k) = 2c_{1212}k^2 + (2f_{122122} + 6f_{122133})k^4. \tag{30}$$

The dynamical matrix of Eq. (29) can be diagonalized to give

$$R^{\text{diag}} = \begin{bmatrix} a(k) + b(k) & 0 & 0 \\ 0 & a(k) - b(k) & 0 \\ 0 & 0 & c(k) \end{bmatrix}. \tag{31}$$

Once again, the above diagonal 3×3 matrix R^{diag} can be compared with the diagonalized acoustic part of the dynamical matrix $\underline{D}^{\text{aa}}(k)|_{3\times3}$ obtained by *ab initio* methods and numerical fitting for different $\mathbf{k}$ vectors can be done to determine the coefficients of k^2 and k^4. A similar procedure can be worked out for wave-vectors along the direction $\mathbf{k} = (1\,1\,1)$. For non-centrosymmetric materials, the procedure remains the same as that for centrosymmetric crystals except that we now must include the contribution of the tensor $\mathbf{d}$ to the phonon-dispersion relations.

In Fig. 2, we show a comparison between the phonon-dispersion curves for copper along [1 0 0] direction obtained by *ab initio* methods to those predicted by strain-gradient elasticity and classical continuum elasticity. The material parameters, including the classical elastic constants and strain-gradient dynamic elastic constants, have been obtained by using the fitting procedure described previously in this section and have been reported in Section 6. Clearly, the phonon dispersion predicted by strain-gradient elasticity

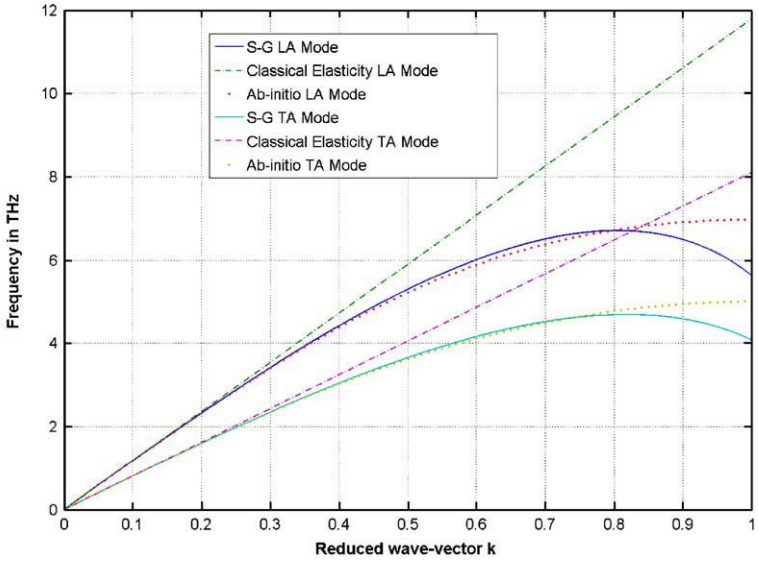

Fig. 2. Shows the comparison of phonon-dispersion curves predicted by strain-gradient elasticity and classical elasticity to those obtained by *ab initio* calculations for the transverse and longitudinal acoustic modes along [1 0 0] direction for copper.

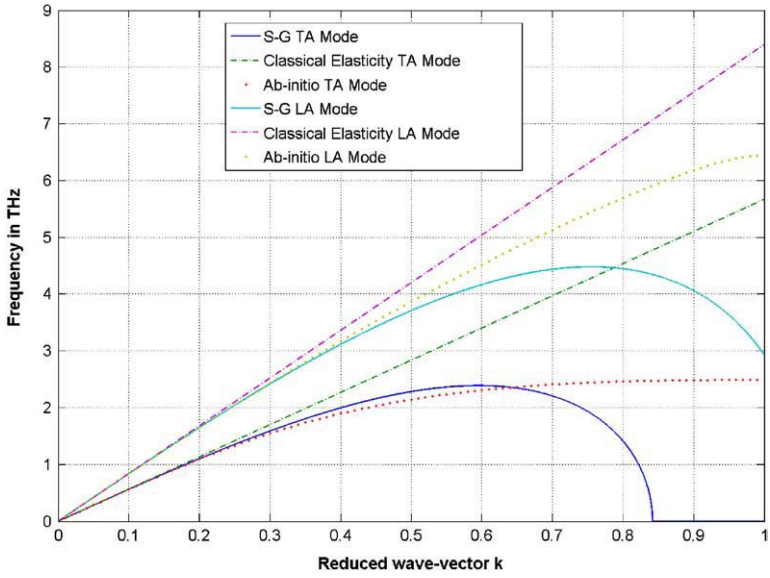

Fig. 3. Shows the comparison of phonon-dispersion curves predicted by strain-gradient elasticity and classical elasticity to those obtained by *ab initio* calculations for the transverse and longitudinal acoustic modes along [1 0 0] direction for gallium arsenide.

matches pretty well to that obtained by *ab initio* calculation over the first half of the Brillouin zone (even though the fitting of the constants has been carried out only for $|k_i| < 0.05$).

The situation is different for GaAs whose phonon-dispersion curves are shown in Fig. 3. The strain-gradient elasticity model can capture the dispersion predicted by *ab initio* calculations only until reduced **k** vector $= (0.2, 0, 0)$ which falls roughly around the 1 THz frequency regime. The failure of the strain-gradient model at higher **k**-vectors for GaAs is more marked than that observed for Cu because of the higher value of dynamic strain-gradient constants of GaAs as compared to Cu.

4. Displacement correlations based MD method for strain-gradient elasticity parameters

In a classical paper by Parrinello and Rahman (1982), it was shown that the fluctuations in elastic strain in a $(\boldsymbol{\sigma}, H, N)$ ensemble (constant stress $\boldsymbol{\sigma}$, constant enthalpy H and constant number of particles N) are a direct measure of the elastic compliances of a general anisotropic medium. Several works based on this approach have appeared since then (Ray, 1983; Ray et al., 1986; Lutsko, 1988; Cagin and Ray, 1988; Gusev et al., 1996; Zhou and Joos, 2002). Ray (1983) provided a systematic derivation of Parrinello and Rahman's technique in a Hamiltonian setting, Lutsko (1988) outlined the technique to investigate crystal properties using local stress fluctuations, Cagin and Ray (1988) used Parrinello and Rahman's techniques to evaluate out non-linear third-order elastic constants. On a related note, Landau and Lifshitz (1984) and later Pratt (1987) outlined a simple technique to determine the elastic constants from atomic displacement correlations. More recently, Meyers et al. (2005) have proposed a methodology based on Pratt's (1987) technique to

determine the classical elastic constants of homogeneous solids from the atomic displacement correlation function in an NVT (constant number of particles N, constant volume V and constant temperature T) MD ensemble using the long-wavelength approximation. In our work, we extend this technique to be applicable in regime of relatively high-energy wave-vectors so that the strain-gradient elasticity constants can be subsequently extracted from the atomic displacement correlation functions. This method proves advantageous over methods involving strain–strain fluctuations (or stress–stress fluctuations) in that it involves atomic displacements which are easily determined during the course of a simulation as opposed to local strain and stress measures.

Consider an elastic solid consisting of "N" atoms contained in a simulation cell of fixed volume "V" that is held at a constant temperature "T". According to the extended continuum strain-gradient elasticity theory, in an elastically homogeneous, stress-free isothermal system, the difference in free energy ΔF between two states with the same N is given by

$$\Delta F = \int_V \frac{C_{ijkl}}{2} u_{i,j}(\mathbf{r}) u_{k,l}(\mathbf{r})\,\mathrm{d}\mathbf{r} + \int_V D_{ijklm} u_{i,j}(\mathbf{r})_{k,lm}(\mathbf{r})\,\mathrm{d}\mathbf{r} + \int_V F^1_{ijklmn} u_{i,jk}(\mathbf{r}) u_{l,mn}(\mathbf{r})\,\mathrm{d}\mathbf{r} + \int_V F^2_{ijklmn} u_{i,j}(\mathbf{r}) u_{k,lmn}(\mathbf{r})\,\mathrm{d}\mathbf{r}. \tag{32}$$

This difference in free energy can be written in a more useful form by introducing the discrete Fourier transform pair

$$\tilde{f}(\mathbf{k}) = \frac{1}{N} \sum_{\alpha=1-N} f^\alpha \exp(-\mathrm{i}\mathbf{k}.\langle \mathbf{r}^\alpha \rangle),$$
$$f^\alpha = \sum_k \tilde{f}(k) \exp(\mathrm{i}\mathbf{k}.\langle \mathbf{r}^\alpha \rangle), \tag{33}$$

where $\mathbf{r}^\alpha$ is the position vector of atom α and $\langle\ \rangle$ denotes a thermal average. Next, we discretize the integral given by Eq. (32)

$$\Delta F = \frac{V}{N} \sum_{\alpha=1-N} \left(\begin{array}{l} C_{ijkl} u_{i,j}(\langle \mathbf{r}^\alpha \rangle) u_{k,l}(\langle \mathbf{r}^\alpha \rangle) + D_{ijklm} u_{i,j}(\langle \mathbf{r}^\alpha \rangle)_{k,lm}(\langle \mathbf{r}^\alpha \rangle) \\ \quad + F^1_{ijklmn} u_{i,jk}(\langle \mathbf{r}^\alpha \rangle) u_{l,mn}(\langle \mathbf{r}^\alpha \rangle) + F^2_{ijklmn} u_{i,j}(\langle \mathbf{r}^\alpha \rangle) u_{k,lmn}(\langle \mathbf{r}^\alpha \rangle) \end{array} \right) \tag{34}$$

and using the Fourier transform defined above we have

$$\Delta F = \frac{V}{N} \sum_{\alpha=1-N} \sum_k \sum_h \left(\begin{array}{l} C_{ijkl} \tilde{u}_{i,j}(\mathbf{h}) \tilde{u}_{k,l}(\mathbf{k}) + D_{ijklm} \tilde{u}_{i,j}(\mathbf{h}) \tilde{u}_{k,lm}(\mathbf{k}) \\ \quad + F^1_{ijlkmn} \tilde{u}_{i,jl}(\mathbf{h}) \tilde{u}_{k,mn}(\mathbf{k}) + F^2_{ijklmn} \tilde{u}_{i,j}(\mathbf{h}) \tilde{u}_{k,lmn}(\mathbf{k}) \end{array} \right) \times \exp[\mathrm{i}(\mathbf{k}+\mathbf{h}).\langle \mathbf{r}^\alpha \rangle]. \tag{35}$$

The summation in Eq. (35) can be further simplified as

$$\Delta F = V \sum_k (C_{ijkl} k_j k_l + i D_{ijklm} k_j k_l k_m + (F^1_{ijlkmn} - F^2_{ijklmn}) k_j k_l k_m k_n) \tilde{u}_i(\mathbf{k}) \tilde{u}_k(-\mathbf{k}). \tag{36}$$

From the symmetries obtained by permuting the k's in Eq. (36) and also by the fact that the above expression contains a factor of the form $\tilde{u}_i(\mathbf{k})\tilde{u}_k(-\mathbf{k})$, Eq. (36) can be

rewritten as

$$\Delta F = V\sum_{k}(c_{ijkl}k_jk_l + id_{ijklm}k_jk_lk_m - f_{ijklmn}k_jk_lk_mk_n)\tilde{u}_i(\mathbf{k})\tilde{u}_k(-\mathbf{k}), \tag{37}$$

where the constants $\mathbf{c}, \mathbf{d}$ and $\mathbf{f}$ possess the exact same symmetries as those in Eqs. (6a–c). Thus, even by employing MD NVT ensemble method we can only extract the *dynamic* elastic constants as in the lattice-dynamics based method.

Now, since the probability of a thermal fluctuation is given by $p \propto \exp[-\Delta F/k_{\mathrm{B}}T]$, one obtains from Gaussian integration:

$$\langle\tilde{u}_i(\mathbf{k})\tilde{u}_k(-\mathbf{k})\rangle = \frac{k_{\mathrm{B}}T}{V}(c_{ijkl}k_jk_l + id_{ijklm}k_jk_lk_m - f_{ijklmn}k_jk_lk_mk_n)^{-1}. \tag{38}$$

If we employ a cubic simulation box with an edge of length L, Eq. (38) can be written as

$$\langle\tilde{u}_i(\mathbf{k})\tilde{u}_k(-\mathbf{k})\rangle = \frac{k_{\mathrm{B}}T}{L^3}(c_{ijkl}k_jk_l + id_{ijklm}k_jk_lk_m - f_{ijklmn}k_jk_lk_mk_n)^{-1}. \tag{39}$$

For a cubic simulation box with periodic boundary conditions, the allowed wave-vectors are of the form $(2\pi/L)(n,p,q)$.

To obtain the requisite dynamic elastic constants from Eq. (39), an NVT MD simulation is carried out at low temperatures for atoms enclosed in a cubic simulation box. The displacements of all the atoms are obtained at each time-step. These displacements in real space can be transformed into Fourier space using Eq. (33) and the correlations given by the left-hand side of Eq. (39) can be calculated for wave-vectors along high-symmetry directions. To achieve nearly independent data samples, the displacement correlations can be tabulated at every 40 time-steps. The thermal average of the displacement correlations can be obtained for different $\mathbf{k}$ vectors and can be fitted to the right-hand side of Eq. (39) to obtain the dynamic elastic constants $\mathbf{c}, \mathbf{d}$ and $\mathbf{f}$. It should be noted that since the fitting of the dynamic elastic constants needs to be carried out in the long-wavelength limit (in the vicinity of $\mathbf{k} = 0$), and since the smallest allowed wave-vector is $2\pi/L$, the length of the simulation box needs to be large enough i.e. we must have a large number of atoms in the periodic simulation cell.[3]

As will be elaborated further in Section 6, in this work the MD simulations for Cu, Al, Ni, Si and SiO_2 have been carried out using the General Lattice Utility Program (GULP) (Gale, 1997; Gale and Rohl, 2003). An embedded atom potential (Cleri and Rosato, 1993) was adopted for the metals Cu, Al and Ni, the Tersoff potential (Tersoff, 1988) was used to carry out MD of the semiconductor Si and the Vashishta potential (Vashishta et al., 1990) was used to simulate SiO_2. MD simulations of the polymers were carried out using the Discover module of Materials Studio® 3.0 using the consistent valence force field (CVFF). Empirical MD simulations for the multi-component semiconductors GaAs and GaP were avoided since reliable inter-atomic potentials are unavailable (and thus only *ab initio* based lattice dynamics was used for these material systems). All the simulations were carried out at a temperature of 50 K. While the convergence of the elastic constants using this method was found to be slower compared to some other works available in the literature (Ray et al. 1985, 1986) (typical runs consisted of 1×10^6 time-steps each time-step being 1 fs), this

[3]A large periodic simulation box is also necessary to eliminate the effect of finite simulation box size. In fact the size of the system being simulated must at least be an order of magnitude larger than the correlation lengths which are typically 2–3 lattice spacings.

method was nevertheless employed since it is quite simple to extend Meyer et al.'s technique (originally due to Pratt, 1987 and Landau and Lifshitz, 1984) to include the effects of strain gradients. Including the effects of strain gradients is not straightforward in other fluctuation-based techniques to calculate elastic constants: for example the Parrinello and Rahman (1982) technique uses a $(\boldsymbol{\sigma}, H, N)$ ensemble wherein a constant external stress is applied and the fluctuations in the strain (which is the conjugate variable to stress) are in turn related to the classical elastic constants. Trying a similar approach to determine the strain-gradient elasticity constants would require application of an external "couple-stress" (which is the conjugate variable to strain gradient): how one can achieve this in a computational ensemble is currently unclear.

In the following section we somewhat digress from this work's central theme of determining the magnitude of the strain-gradient constants to discuss the issue of the sign of the *dynamic* strain-gradient elasticity constants required to make strain-gradient theory thermodynamically stable while requiring to correctly predict observed dispersion of phonon curves.

5. The "sign" paradox

Though strain-gradient elasticity theories have enjoyed increased attention in recent years, some confusion still exists over the sign of the strain-gradient constants required for uniqueness and that required to explain the dispersive character of phonons when a straightforward extension of a simple strain-gradient elasticity model is made to dynamics.

Consider a simple one-dimensional strain-gradient elasticity model (Yang and Guo, 2005) where the elastic energy density U takes the form

$$U = \tfrac{1}{2}[a(u')^2 + 2bu'u'' + c(u'')^2]. \tag{40}$$

For thermodynamic stability, U is required to be positive definite which implies the following constraints:

$$a > 0, \quad c > 0 \quad \text{and} \quad ac > b^2. \tag{41}$$

The equation of motion from Eq. (35) can be determined variationally as being

$$\rho\ddot{u} = au'' - cu''''. \tag{42}$$

To obtain the dispersion relation one may substitute a plane wave equation with frequency ω and wave-vector $\mathbf{k}$ for the displacement $\mathbf{u}$ as $u_i = u_i^0 \exp \mathrm{i}(\omega t + \mathbf{k}\cdot\mathbf{r})$. After carrying out this substitution, the dispersion relation becomes

$$\rho\omega^2 = ak^2 + ck^4. \tag{43}$$

Invoking the restrictions on the material constants of Eq. (45), one can see from Eq. (43) that the dispersion curves will curve upwards with increasing $\mathbf{k}$, which is in direct conflict with most experimentally observed phonon-dispersion curves which tend to dip downwards with increasing $\mathbf{k}$, thereby rendering the coefficient of the k^4 term in the dispersion relation to be negative. Notice that in the aforementioned model, the static strain-gradient constant of Eq. (40) is equal to the dispersive elastic constant of Eq. (43).

Several other works have discussed this issue most notable of them being Askes et al. (2002), Metrikine and Askes (2002a, b), Chang et al. (2003a,b), Borino and Polizzotto (2003). More recently Askes and Aifantis (2006) have suggested inclusion of a higher-order inertial term to

the equations of motion derived from strain-gradient elasticity so that the theory is both thermodynamically stable and is also able to explain the observed dispersive phenomena.

Part of the confusion probably arises due to the extreme simplicity of the strain-gradient models that are typically used. In the simple model used by Yang and Guo (2005), the k^4 dispersive contribution to the phonon-dispersion relation arises only due to the strain-gradient coupling terms (in Eq. (40)). Since this coupling is biquadriatic in nature, the coupling constant c is restricted by thermodynamic considerations to assume positive values. On the other hand, in our model (where all admissible couplings are included), the dispersive elastic constant $\mathbf{f}$ is a linear combination of the static elastic constants $\mathbf{F}^1$ and $\mathbf{F}^2$.

$$f_{ijklmn} = \mathrm{sym}_{(i,k)}\mathrm{sym}_{(j,l,m,n)}(F^2_{ijklmn} - F^1_{ijlkmn}). \tag{44}$$

So even though, the tensor $\mathbf{F}^1$ (which couples strain-gradients to strain-gradients) is required to be positive definite, there is no such restriction on the tensor $\mathbf{F}^2$ (which couples strains to second gradients of strain) and the tensor $\mathbf{f}$ can be such that the continuum model given by the Lagrangian of Eq. (1) can remain thermodynamically stable and also be able to model the observed dispersive effects.

6. Numerical results for various materials

In this section we present the values of the dynamic strain-gradient constants obtained for various materials by employing the techniques discussed in Sections 3 and 4. For the fcc metals Cu and Al we have employed both *ab initio* lattice dynamics and our fluctuation-based empirical MD simulation method. For Si we have employed all the three methods i.e. *ab initio* and empirical lattice dynamics and empirical MD. For C (diamond) and GaAs we have used *ab initio* and empirical lattice dynamics to estimate the dispersive constants while for Ge and GaP we have used only empirical lattice dynamics (due to the lack of availability of faithful atomistic potentials). Lastly, for the non-crystalline systems investigated viz. amorphous silica and polythene only our fluctuation-based MD method is applicable.

6.1. Copper

Ab initio phonon dispersions of Cu were calculated within density-functional perturbation theory in the generalized gradient approximation (GGA). An ultrasoft pseudopotential generated by Favot and Dal Corso (1999) using an approach outlined by Kresse and Hafner (1994) was employed. The core radii (in atomic units a.u.) of the pseudopotential employed was 3*d* (1.7, 2.2) 4*p* (2.8) local-4*s* (2.8) (refer to Favot and Dal Corso, 1999). A kinetic energy cut-off of 30 Rydbergs (Ry) was chosen and the augmentation charges were expanded to 300 Ry as suggested by Favot and Dal Corso (1999). For the BZ integration 60 $\mathbf{q}$ points in the irreducible BZ were used and the integration up to the Fermi surface was done with the Methfessel–Paxton technique implemented in Quantum-ESPRESSO with a smearing parameter $\boldsymbol{\sigma} = 0.05$ Ry. The dynamical matrices were generated on an $8 \times 8 \times 8$ $\mathbf{k}$-point mesh, and Fourier interpolation implemented in Quantum-ESPRESSO was used to obtain the complete phonon-dispersion curves.

The *NVT* MD for Cu were carried out employing the Cleri–Rosato EAM potential using GULP. A periodic simulation cell containing 4000 atoms was employed along with

Table 1
Non-dispersive and dispersive elastic constants of copper obtained from *ab initio* lattice dynamics and empirical molecular dynamics (MD) using the EAM potential

	Ab initio lattice dynamics	MD	Experiment
c_{1111} (dyn/cm^2) ($\times 10^{12}$)	1.62	1.75	1.66
$c_{1212}(\times 10^{12})$	0.76	0.81	0.76
$c_{1122}(\times 10^{12})$	1.18	1.23	1.19
f_{111111} (dyn) ($\times 10^{-4}$)	0.41	0.60	
$f_{122122}(\times 10^{-4})$	0.19	0.22	
$f_{211222}(\times 10^{-4})$	0.27	0.29	
$f_{112222}(\times 10^{-4})$	0.33	0.34	
$f_{122133}(\times 10^{-4})$	0.07	−0.03	
$f_{112233}(\times 10^{-4})$	0.06	0.02	

Nosé–Hoover dynamics to maintain a constant temperature of 50 K. After equilibration, the displacement correlations were tabulated every 40 time-steps (each time-step being 1 fs): the simulation was allowed to run for 1 ns (1 million time-steps). The results obtained for the dynamic strain-gradient constants for Cu have been listed in Table 1. Using the *ab initio* results obtained in Table 1, the non-local length scales for Cu along the longitudinal and transverse directions become 0.5 Å each.

6.2. Aluminum

Ab initio phonon dispersions of Al were calculated in the GGA using a norm-conserving pseudopotential generated by Favot and Dal Corso (1999) following the Rappe, Rabe, Kaxiras and Joannopoulos scheme. The core radii of the pseudopotential used was 3*s* (2.7) 3*p*(2.7) local-3*d*(2.7). A kinetic energy cut-off of 20 Ry was chosen as suggested by Favot and Dal Corso (1999). For the BZ integration 60 **q** points were used; the smearing technique employed was similar to that of Cu. The dynamical matrices were again generated on an $8 \times 8 \times 8$ **k**-point mesh, and Fourier interpolation was carried out to obtain the complete phonon-dispersion curves.

The NVT MD for Al were carried out in a manner similar to that of Cu using the Cleri–Rosato EAM potential employing GULP. The results obtained for the dynamic strain-gradient constants for Al have been listed in Table 2.

Using the *ab initio* results obtained, the non-local length scales along the longitudinal and transverse directions are 0.9 and 1.22 Å, respectively.

6.3. Silicon

Ab initio phonon dispersions of Si were calculated in the GGA using a norm-conserving pseudopotential generated by Favot et al. following the Rappe, Rabe, Kaxiras and Joannopoulos scheme. The core radii of the pseudopotential used was 3*s* (2.5) 3*p*(2.5) local-3*d*(2.5). A kinetic energy cut-off of 24 Ry was chosen as suggested by Favot and Dal Corso (1999). For the BZ integration 60 **q** points were used. The dynamical matrices were generated on an $8 \times 8 \times 8$ **k**-point mesh, and Fourier interpolation was carried out to obtain the complete phonon-dispersion curves.

Table 2
Non-dispersive and dispersive elastic constants of aluminum obtained from *ab initio* lattice dynamics and empirical molecular dynamics (MD) using the EAM potential

	Ab initio lattice dynamics	MD	Experiment
c_{1111} (dyn/cm^2)($\times 10^{12}$)	1.10	0.945	1.09
$c_{1212}(\times 10^{12})$	0.30	0.37	0.30
$c_{1122}(\times 10^{12})$	0.64	0.74	0.64
f_{111111} (dyn) ($\times 10^{-4}$)	0.87	0.60	
$f_{122122}(\times 10^{-4})$	0.45	0.13	
$f_{211222}(\times 10^{-4})$	−0.17	0.22	
$f_{112222}(\times 10^{-4})$	−0.04	0.27	
$f_{122133}(\times 10^{-4})$	0.53	−0.02	
$f_{112233}(\times 10^{-4})$	0.08	0.04	

Table 3
Non-dispersive and dispersive elastic constants of silicon obtained from *ab initio* lattice dynamics, empirical Shell Model lattice dynamics and empirical molecular dynamics (MD) using the Tersoff potential

	Ab initio lattice dynamics	Lattice dynamics: Shell Model	MD	Experiment
c_{1111}(dyn/cm^2)($\times 10^{12}$)	1.68	1.66	1.45	1.66
$c_{1212}(\times 10^{12})$	0.81	0.80	0.70	0.796
$c_{1122}(\times 10^{12})$	0.63	0.64	0.77	0.64
f_{111111} (dyn) ($\times 10^{-4}$)	2.9	0.39	0.37	0.36
$f_{122122}(\times 10^{-4})$	4.1	2.7	0.27	
$f_{211222}(\times 10^{-4})$	0.84	0.48	0.34	
$f_{112222}(\times 10^{-4})$	0.67	0.06	0.32	
$f_{122133}(\times 10^{-4})$	−0.42	0.48	−0.19	
$f_{112233}(\times 10^{-4})$	−0.66	−0.24	−0.10	

The experimental data for the dispersive elastic constant f_{111111} are from Hao and Maris (2000, 2001).

For the empirical lattice dynamics, Shell Model parameters for Si provided by Price et al. (1971) were used (also see Kunc and Nielsen, 1979a, b). The NVT MD for Si were carried out employing the Tersoff potential using GULP. A periodic simulation cell containing 4096 atoms was employed along with Nosé–Hoover dynamics to maintain a constant temperature of 50 K. After equilibration, the displacement correlations were tabulated every 40 time-steps (each time-step being 1 fs): the simulation was allowed to run for 1 ns (1 million time-steps). The results obtained for the dynamic strain-gradient constants for Si have been listed in Table 3.

Using the *ab initio* results obtained, the non-local length scales along the longitudinal and transverse directions are 1.3 and 2.25 Å, respectively.

6.4. Germanium

The empirical lattice dynamics of germanium were carried out using the Shell Model parameters provided by Price et al. (1971). The results obtained for the dynamic strain-gradient constants for Ge have been listed in Table 4.

Table 4
Non-dispersive and dispersive elastic constants of germanium obtained from empirical Shell Model lattice dynamics

	Lattice dynamics: Shell Model	Experiment
$c_{1111}(\text{dyn/cm}^2)(\times 10^{12})$	1.31	1.26
$c_{1212}(\times 10^{12})$	0.68	0.677
$c_{1122}(\times 10^{12})$	0.49	0.44
f_{111111} (dyn) $(\times 10^{-4})$	0.08	0.58
$f_{122122}(\times 10^{-4})$	2.52	
$f_{211222}(\times 10^{-4})$	0.03	
$f_{112222}(\times 10^{-4})$	0.01	
$f_{122133}(\times 10^{-4})$	0.63	
$f_{112233}(\times 10^{-4})$	−0.29	

The experimental data for the dispersive elastic constant f_{111111} are from Hao and Maris (2001).

Table 5
Non-dispersive and dispersive elastic constants of diamond obtained from *ab initio* and empirical Shell Model lattice dynamics

	Ab initio lattice dynamics	Lattice dynamics: Shell Model	Experiment
$c_{1111}(\text{dyn/cm}^2)(\times 10^{12})$	10.72	10.78	10.79
$c_{1212}(\times 10^{12})$	5.70	5.77	5.78
$c_{1122}(\times 10^{12})$	1.23	1.25	1.24
f_{111111} (dyn) $(\times 10^{-4})$	2.39	2.52	
$f_{122122}(\times 10^{-4})$	1.60	2.60	
$f_{211222}(\times 10^{-4})$	1.87	1.65	
$f_{112222}(\times 10^{-4})$	1.21	0.12	
$f_{122133}(\times 10^{-4})$	−0.17	0.76	
$f_{112233}(\times 10^{-4})$	−0.82	−0.15	

Using the empirical lattice dynamics results obtained, the non-local length scales along the longitudinal and transverse directions are 0.25 and 1.92 Å, respectively.

6.5. Diamond (C)

Ab initio phonon dispersions of diamond were calculated in the GGA using an ultrasoft pseudopotential generated by Favot et al. using an approach outlined by Kresse and Hafner (1994). The core radii of the pseudopotential used was 2*s* (1.2, 1.6) 2*p*(1.3, 1.7) local-3*d*(1.7). A kinetic energy cut-off of 28 Ry was chosen and the augmentation charges were expanded to 220 Ry as suggested by Favot and Dal Corso (1999). For the BZ integration 28 **q** points were used. The dynamical matrices were generated on an $8 \times 8 \times 8$ **k**-point mesh, and Fourier interpolation was carried out to obtain the complete phonon-dispersion curves. For the empirical lattice dynamics, Shell Model parameters for diamond provided by Price et al. (1971) were used. The results obtained for the dynamic strain-gradient constants have been listed in Table 5.

Table 6
Non-dispersive and dispersive elastic constants of gallium arsenide obtained from *ab initio* and empirical Shell Model and Dipole Model lattice dynamics

	Ab initio lattice dynamics	Lattice dynamics: Shell Model	Lattice dynamics: Dipole Model	Experiment
c_{1111}(dyn/cm^2)($\times 10^{12}$)	1.17	1.20	1.19	1.18
$c_{1212}(\times 10^{12})$	0.56	0.57	0.57	0.56
$c_{1122}(\times 10^{12})$	0.59	0.60	0.60	0.59
d_{12223} (dyn/cm) ($\times 10^3$)	−1.3	−1.8	−4.1	
f_{111111} (dyn) ($\times 10^{-4}$)	0.40	0.26	0.40	0.36
$f_{122122}(\times 10^{-4})$	1.08	2.04	1.05	
$f_{211222}(\times 10^{-4})$	0.22	0.24	0.25	
$f_{112222}(\times 10^{-4})$	0.24	0.16	0.03	
$f_{122133}(\times 10^{-4})$	0.94	0.48	0.45	
$f_{112233}(\times 10^{-4})$	0.02	−0.19	−0.08	

The experimental data for the dispersive elastic constant f_{111111} are from Hao and Maris (2001).

Using the *ab initio* results obtained, the non-local length scales along the longitudinal and transverse directions are 0.47 and 0.53 Å, respectively.

6.6. Gallium arsenide

Ab initio phonon dispersions of GaAs were calculated in the local density approximation (LDA) using a norm-conserving pseudopotential generated by Giannozzi et al. (1991) following a scheme proposed by von Barth and Car. A kinetic energy cut-off of 25 Ry was chosen and 60 **q** points were used for the BZ integration. An equilibrium lattice parameter of 10.605 a.u. as suggested by Giannozzi et al. was chosen. The dynamical matrices were generated on an $8 \times 8 \times 8$ **k**-point mesh, and Fourier interpolation was carried out to obtain the complete phonon-dispersion curves.

Parameters for the lattice-dynamical models have been taken from Kunc et al. (1975a, b) (also see Kunc and Nielsen, 1979a, b).The results obtained for the dynamic strain-gradient constants for GaAs have been listed in Table 6.

Using the *ab initio* results obtained, the non-local length scales along the longitudinal and transverse directions are 0.49 and 1.4 Å, respectively.

6.7. Gallium phosphide

Parameters for the lattice-dynamical Shell Model for GaP have been taken from Kunc et al. (1975a, b). The results obtained for the dynamic strain-gradient constants have been listed in Table 7.

Using the empirical lattice dynamics results obtained, the non-local length scales along the longitudinal and transverse directions are 0.8 and 1.3 Å, respectively.

Table 7
Non-dispersive and dispersive elastic constants of gallium phosphide obtained from empirical Shell Model lattice dynamics

	Lattice dynamics: Shell Model	Experiment
c_{1111}(dyn/cm^2)($\times 10^{12}$)	1.46	1.405
$c_{1212}(\times 10^{12})$	0.623	0.62
$c_{1122}(\times 10^{12})$	0.707	0.703
d_{12223} (dyn/cm) ($\times 10^{3}$)	−1.3	
f_{111111} (dyn) ($\times 10^{-4}$)	0.90	
$f_{122122}(\times 10^{-4})$	1.07	
$f_{211222}(\times 10^{-4})$	0.39	
$f_{112222}(\times 10^{-4})$	0.35	
$f_{122133}(\times 10^{-4})$	0.37	
$f_{112233}(\times 10^{-4})$	0.03	

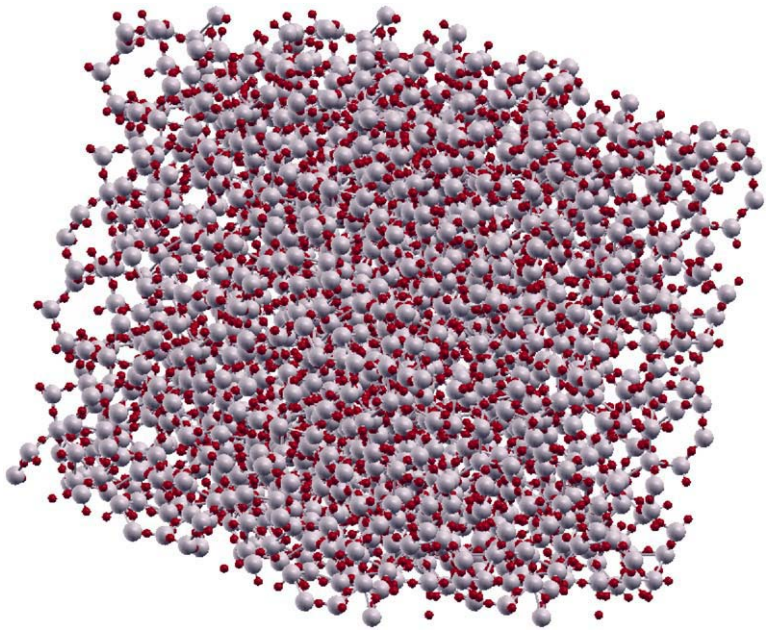

Fig. 4. System of amorphous silica consisting of 5184 atoms confined inside a cubic simulation box used to perform NVT molecular dynamics is shown above. Red balls represent oxygen atoms while gray balls represent silicon atoms.

6.8. Silica

NVT MD on a system of amorphous silica (density 2.2 g/cc) consisting of 5184 atoms in a cubic simulation cell (each side measuring 4.28 nm) was performed under periodic boundary conditions (Fig. 4). A potential developed by Vashishta et al. (1990) was used to

Table 8
Isotropic non-dispersive and dispersive elastic constants of silica obtained from NVT molecular dynamics (MD)

	MD
c_{1111}(dyn/cm^2)($\times 10^{12}$)	1.20
c_{1212}($\times 10^{12}$)	0.54
f_{111111} (dyn) ($\times 10^{-3}$)	0.21
f_{122122}($\times 10^{-3}$)	4.37

perform the MD. Nosé–Hoover dynamics were employed to maintain a constant temperature of 50 K. After equilibration, the displacement correlations were tabulated every 40 time-steps (each time-step being 1 fs): the simulation was allowed to run for 1.5 ns to allow the elastic constants to converge.

The obtained elastic constants are reported in Table 8.

The corresponding length scales for the longitudinal and transverse directions are 1.32 and 9 Å, respectively.

6.9. Polythene

NVT MD on a polythene system (density of 0.75 g/cc) consisting of 38 000 atoms in a cubic simulation cell (with each side measuring 7.35 nm) was performed under periodic boundary conditions (Fig. 5). The CVFF potential was employed and Nosé–Hoover dynamics were employed to maintain a constant temperature of 50 K. After equilibration, the displacement correlations were tabulated every 40 time-steps (each time-step being 1 fs): the simulation was allowed to run for 1.5 ns to allow for the elastic constants to converge.

We report the isotropic constants in Table 9.

The corresponding length scales for the longitudinal and transverse directions are 1.85 and 3.81 nm, respectively.

7. Discussion and relevance for nanotechnologies

In light of the results obtained for the dynamic strain-gradient constants and associated length scales for the materials investigated in the previous section, there seems to be a strong indication that strain-gradient elasticity may be of practical importance only for materials possessing a non-homogeneous microstructure like amorphous silica and polymers. In other words, we believe that non-local, and in particular, strain-gradient elasticity is largely *irrelevant* for most material systems except at impossibly small sizes.[4] As evident, polymers and amorphous materials appear to be the exceptions. Covalent semiconductors like Si, however, possess higher non-local length scales compared to metals which may be attributed to the short-ranged nature of inter-atomic forces in metal.

[4]Although in some cases, even though the length scale is small, non-local effects may be of interest. For example, in quantum dots, see the work of Zhang and Sharma (2005b) although that work used a rather large length scale for GaAs which is refuted by the present work.

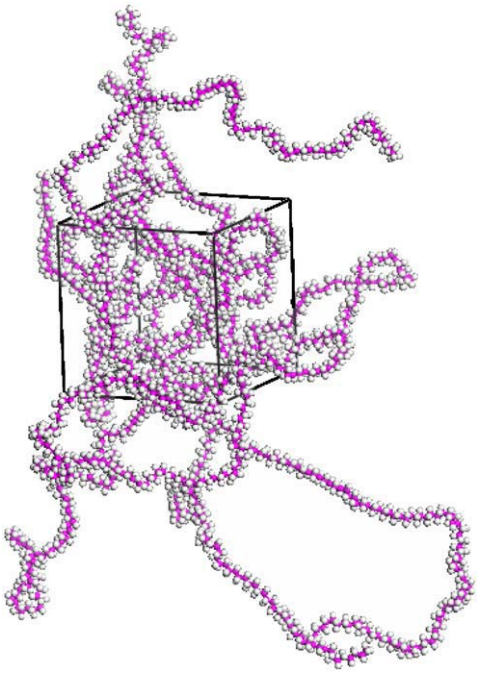

Fig. 5. Shown is a polythene system consisting of 4808 atoms. The pink backbone consists of carbon atoms while the hydrogen atoms are rendered in white.

Table 9
Isotropic non-dispersive and dispersive elastic constants of polythene obtained from NVT molecular dynamics (MD)

	MD
$c_{1111}(\text{dyn/cm}^2)(\times 10^{10})$	0.70
$c_{1212}(\times 10^{10})$	0.31
f_{111111} (dyn) $(\times 10^{-3})$	0.24
$f_{122122}(\times 10^{-3})$	0.45

The high non-locality in amorphous solids possessing an underlying inhomogenous microstructure possibly stems from a group of strongly bonded atoms behaving as a unit. Under such circumstances, parts of the material system may undergo considerable *non-affine* deformation and high moment stresses may result. Since crystalline materials are highly ordered, they very possibly undergo negligible *non-affine* deformations as a consequence of which the strain-gradient effects are unimportant for such systems. Consequently, for such amorphous systems, taking strain-gradient effects into account while investigating nanoscale elastic phenomena may impart significant size-dependent corrections to the results obtained from classical continuum elasticity. These observations agree well with existing literature at hand (Ding et al., 2001; Espinosa et al., 2003; Lam et al., 2003; McFarland and Colton, 2005; Leonforte et al., 2005, 2006). Indeed, experimental

evidence suggests that materials like epoxy resins have length scale of 10 μm (Lam et al., 2003). Liquid-crystal elastomers have also been investigated under the context of Frank elasticity and experimental evidence suggests that their length scales may lie in the 10 nm regime (Warner, 2003). Even for polypropylene McFarland and Colton (2005) have reported a length scale of 10 μm. Our MD simulations for polythene, however, predict a much lower length scale of ~4 nm. We are unable to explain this discrepancy and suspect either presence of a higher-length microstructure or simply because of material difference. The latter assertion is strengthened by the fact that careful experiments on size effects on polystyrene by Stafford et al. (2004)—through two different methods: thin-film wrinkling and nano-indentation—did not reveal any size effects down to 150 nm. A recent work by Nikolov et al. (2006) estimated (based on a simple but elegant micromechanical model) that rubbers should have non-local length scale in the neighborhood of 4.5 nm. The reasons for the high length scales obtained by Lam et al. (2003) for epoxy and by McFarland and Colton (2005) for polypropylene, are somewhat uncertain and require further investigation.

To gauge the magnitude of corrections that strain-gradient effects may impart to results obtained by classical continuum elasticity, we analyze the bending of a beam based on a modified couple-stress theory recently proposed by Park and Gao (2006). A plot of the bending rigidity (normalized with respect to the bending rigidity obtained using the classical Bernoulli–Euler model) versus the beam dimensions provides an illustrative example (Fig. 6). The plot depicts results for polythene and silica using the length scale constants obtained in the previous section. As expected from Park and Gao's (2006)

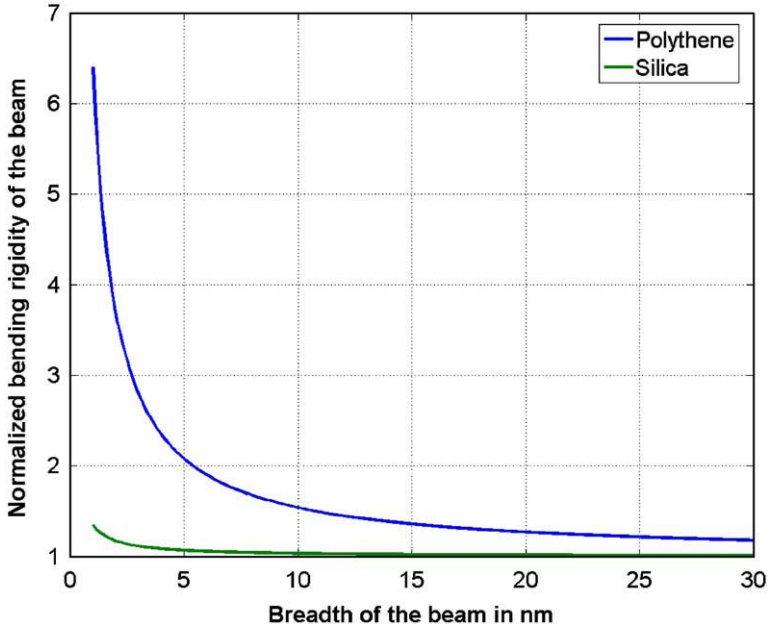

Fig. 6. Bending rigidity of a beam with a rectangular cross-section obtained from a couple-stress model (normalized with respect to the bending rigidity of the beam using the classical Bernoulli–Euler model) versus the breadth of the beam. The height of the beam is the same as the breadth while the length of the beam is 10 times the breadth.

model, there is marked stiffening of the beam with decrease in size. For polythene, in particular, the bending rigidity is double that of the classical bending rigidity at beam dimensions of 5 nm. For silica, the effect is smaller with the bending stiffness being 10% higher than corresponding classical value at dimensions comparable to 5 nm.

We conclude this section with a simple word of caution. Although our results appear to indicate that strain-gradient elasticity is irrelevant for most crystalline metals and ceramics, we wish to point out that under certain circumstances, strain-gradient elasticity is quite useful even in materials exhibiting small non-local characteristic length scales e.g. in analysis of defects. In this regard see the recent work of Zhang et al. (2006) who have shown the utility of using non-local elasticity for the analysis of defects in graphene. Finally, as already alluded to in Section 1, materials with a microstructure such as foams or composites may be fruitfully modeled using strain-gradient elasticity. Our results are only applicable to pure materials that do not contain any "artificial" structural features. Our newly introduced displacement fluctuation correlations based MD method to evaluate strain-gradient elasticity constants is expected to be a powerful tool to explore the non-local size effects in various other materials and systems not tackled in the present work e.g. composites, different classes of polymers and amorphous materials and defective solids.

Acknowledgments

Financial support from ONR Young Investigator award—N000140510662 is gratefully acknowledged. One of the authors (R.M.) would like to thank Xinyuan Zhang for bringing fluctuation-based techniques (to calculate material properties) to his attention. Computational facilities provided by the Texas Learning and Computation Center (TLC2) at the University of Houston are highly appreciated.

References

Aifantis, E.C., 1999. Strain gradient interpretation of size effects. Int. J. Fract. 95, 299–314.

Askes, H., Aifantis, E.C., 2006. Gradient elasticity theories in statics and dynamics—a unification of approaches. Int. J. Fract. 139, 297–304.

Askes, H., Suiker, A.S.J., Sluys, L.J., 2002. A classification of higher-order strain-gradient models—linear analysis. Arch. Appl. Mech. 72, 171–188.

Bamzai, A.S., Deb, B.M., 1981. The role of single-particle density in chemistry. Rev. Mod. Phys. 53, 95–126.

Baroni, S., Giannozzi, P., Testa, A., 1987. Green's-function approach to linear response in solids. Phys. Rev. Lett. 58, 1861–1864.

Baroni, S., de Gironcoli, S., Dal Corso, A., Giannozzi, P., 2001. Phonons and related crystal properties from density-functional perturbation theory. Rev. Mod. Phys. 73, 515–562.

Borino, G., Polizzotto, C., 2003. Paper: "Higher-order strain/higher-order stress gradient models derived from a discrete microstructure, with application to fracture," by C.S. Chang, H. Askes and L.J. Sluys; Engineering Fracture Mechanics 69 (2002), 1907–1924. Eng. Fract. Mech. 70, 1219–1221.

Bouyge, F., Jasiuk, I., Ostoja-Starzewski, M., 2001. A micromechanically based couple-stress model of an elastic two-phase composite. Int. J. Solids Struct. 38 (10–13), 1721–1735.

Cagin, T., Ray, J.R., 1988. Third-order elastic constants from molecular dynamics: theory and an example calculation. Phys. Rev. B 38, 7940–7946.

Cammarata, R.C., Sieradzki, K., 1994. Surface and interface stresses. Ann. Rev. Mater. Sci. 24, 215–234.

Chang, C.S., Askes, H., Sluys, L.J., 2003a. Higher-order strain/higher-order stress gradient models derived from a discrete microstructure, with application to fracture. Eng. Fract. Mech. 69, 1907–1924.

Chang, C.S., Askes, H., Sluys, L.J., 2003b. Reply to letter to the editor as written by G. Borino and C. Polizzotto. Eng. Fract. Mech. 70, 1223–1224.

Chen, Y., Lee, J.D., Eskandarian, A., 2003. Examining the physical foundation of continuum theories from the viewpoint of phonon dispersion relation. Int. J. Eng. Sci. 41, 61–83.
Chen, Y., Lee, J.D., Eskandarian, A., 2004. Atomistic viewpoint of the applicability of microcontinuum theories. Int. J. Solids Struct. 41, 2085–2097.
Cheng, Z.Q., He, L.H., 1995. Micropolar elastic fields due to a spherical inclusion. Int. J. Eng. Sci. 33, 389–397.
Cheng, Z.Q., He, L.H., 1997. Micropolar elastic fields due to a circular cylindrical inclusion. Int. J. Eng. Sci. 35, 659–668.
Cleri, F., Rosato, V., 1993. Tight-binding potentials for transition metals and alloys. Phys. Rev. B 48, 22–33.
Ding, J.N., Meng, Y.G., Wen, S.Z., 2001. Specimen size effect on mechanical properties of polysilicon microcantilever beams measured by deflection using a nanoindenter. Mater. Sci. Eng. B 83, 42–47.
DiVincenzo, D.P., 1986. Dispersive corrections to continuum elastic theory in cubic crystals. Phys. Rev. B. 34, 5450–5465.
Drugan, W.J., 2000. Micromechanics-based variational estimates for a higher-order non-local constitutive equation and optimal choice of effective moduli for elastic composites. J. Mech. Phys. Solids 48, 1359–1387.
Duan, H.L., Wang, J., Huang, Z.P., Karihaloo, B.L., 2005. Eshelby formalism for nano-inhomogeneities. Proc. R. Soc. A 461, 3335–3353.
Eringen, A.C., 1999. Microcontinuum Field Theories. I: Foundations and Solids. Springer, New York.
Eringen, A.C., Edelen, D.G.B., 1972. On nonlocal elasticity. Int. J. Eng. Sci. 10, 233–248.
Espinosa, H.D., Prorok, B.C., Peng, B., Kim, K.H., Moldovan, N., Auciello, O., Carlisle, J.A., Gruen, D.M., Mancini, D.C., 2003. Mechanical properties of ultrananocrystalline diamond thin films relevant to MEMS devices. Exp. Mech. 43, 256–268.
Every, A.G., 2005. Weak spatial dispersion and the unfolding of wave arrival singularities in the elastodynamic Green's functions of solids. Phys. Rev. B 72, 104302-1–104302-10.
Fatemi, J., Van Keulen, F., Onck, P., 2002. Generalized continuum theories: application to stress analysis in bone. Meccanica 37 (4–5), 385–396.
Favot, F., Dal Corso, A., 1999. Phonon dispersions: Performance of the generalized gradient approximation. Phys. Rev. B 60, 427–431.
Forest, S., Barbe, F., Cailletaud, G., 2000. Cosserat modelling of size effects in the mechanical behaviour of polycrystals and multi-phase materials. Int. J. Solids Struct. 37 (46–47), 7105–7126.
Frantziskonis, G., Aifantis, E.C., 2002. On the stochastic interpretation of gradient-dependent constitutive equations. Eur. J. Mech. A 21, 589–596.
Gale, J.D., 1997. GULP—a computer program for the symmetry adapted simulation of solids. J. Chem. Soc. Faraday Trans. 93, 629.
Gale, J.D., Rohl, A.L., 2003. The general utility lattice program. Mol. Simulat. 29, 291–341.
Giannozzi, P., de Gironcoli, S., Pavone, P., Baroni, S., 1991. Ab-initio calculation of phonon dispersions in semiconductors. Phys. Rev. B 43, 7231–7242.
Green, A.E., Rivlin, R.S., 1964. The mechanics of materials with structure. Technical Report No. 94, NTIS.
Groma, I., Csikor, F.F., Zaiser, M., 2003. Spatial correlations and higher-order gradient terms in a continuum description of dislocation dynamics. Acta Mater. 51, 1271–1281.
Gurtin, M.E., Murdoch, A.I., 1975. A continuum theory of elastic material interfaces. Arch. Rat. Mech. Anal. 57, 291–323.
Gurtin, M.E., Murdoch, A.I., 1978. Surface stress in solids. Int. J. Solids Struct. 14, 431–440.
Gusev, A.A., Zehnder, M.M., Suter, U.W., 1996. Fluctuation formula for elastic constants. Phys. Rev. B 54, 54–57.
Gutkin, M.Yu., 2000. Nanoscopics of dislocations and disclinations in gradient elasticity. Rev. Adv. Mater. Sci. 1, 34.
Gutkin, M.Yu., Aifantis, E.C., 1999. Dislocations and disclinations in gradient elasticity. Phys. Stat. Sol. B 214, 245–284.
Hao, H.-Y., Maris, H.J., 2000. Study of phonon dispersion in silicon and germanium at long wavelengths using picosecond ultrasonics. Phys. Rev. Lett. 84, 5556–5559.
Hao, H.-Y., Maris, H.J., 2001. Dispersion of the long-wavelength phonons in Ge, Si, GaAs, quartz and sapphire. Phys. Rev. B 63, 224301–224310.
He, L.H., Lim, C.W., Wu, B.S., 2004. A continuum model for size-dependent deformation of elastic films of nano-scale thickness. Int. J. Solids Struct. 41, 847–857.
Hohenberg, P., Kohn, W., 1964. Inhomogeneous electron gas. Phys. Rev. 136, 864–871.
Kleinert, H., 1989. Gauge Fields in Condensed Matter, vol. 2. World Scientific, Singapore ISBN 9971-50-210-0.

Kohn, W., Sham, L.J., 1965. Self-consistent equations including exchange and correlation effects. Phys. Rev. 140, A1133–A1138.
Koiter, W.T., 1964. Couple stresses in the theory of elasticity. I and II. P. K. Ned. Akad. Wetensc. B 67, 17–44.
Kresse, G., Hafner, J., 1994. Norm-conserving and ultrasoft pseudopotentials for first-row and transition elements. J. Phys. Condens. Mater. 6, 8245–8257.
Kroner, E., 1970. The problem of non-locality in the mechanics of solids: review on present status. In: Proceedings of the Conference on Fundamental Aspects of Dislocation Theory, pp. 729–736.
Krumhansl, J.A., Kroner, E., 1968. Mechanics of Generalized Continua. Springer, Berlin.
Kukta, R., Peralta, A., Kouris, D., 2002. Surface steps: from atomistics to continuum. ASME J. Appl. Mech. 69, 443–450.
Kunc, K., Nielsen, O.H., 1979a. Lattice dynamics of zincblende structure compounds using deformation-dipole model and rigid ion model. Comp. Phys. Commun. 16, 181–197.
Kunc, K., Nielsen, O.H., 1979b. Lattice dynamics of zincblende structure compounds II. Shell model. Comp. Phys. Commun. 17, 413–422.
Kunc, K., Balkanski, M., Nusimovici, M., 1975a. Lattice dynamics of several AN-B8-N compounds having the Zincblende structure. Pt. 1. Deformable-bond approximation. Phys. Status Solidi B 71, 341–349.
Kunc, K., Balkanski, M., Nusimovici, M., 1975b. Lattice dynamics of several AN-B8-N compounds having the zincblende structure. Pt. 2. Numerical calculations. Phys. Status Solidi B 72, 229–248.
Kunin, I., 1982. Quantum mechanical formalism in classical wave propagation problems. Int. J. Eng. Sci. 20, 271–280.
Kunin, I., 1984. On foundations of the theory of elastic media with microstructure. Int. J. Eng. Sci. 22, 969–978.
Lam, D.C.C., Yang, F., Chong, A.C.M., Wang, J., Tong, P., 2003. Experiments and theory in strain gradient elasticity. J. Mech. Phys. Solids 51, 1477–1508.
Landau, L.D., Lifshitz, E.M., 1984. Statistical Physics. Part 1. Course of Theoretical Physics, vol. 5. Butterworths, London.
Lax, M., 1974. Symmetry Principles in Solid State and Molecular Physics. Wiley, New York.
Leonforte, F., Boissiere, R., Tanguy, A., Wittmer, J.P., Barrat, J.-L., 2005. Continuum limit of amorphous elastic bodies. III. Three-dimensional systems. Phys. Rev. B 72, 224206–224217.
Leonforte, F., Tanguy, A., Wittmer, J.P., Barrat, J.-L., 2006. Inhomogeneous elastic response of silica glass. Phys. Rev. Lett. 97, 055501–055504.
Li, L.Y., Dunn, M.L., 1998. Anisotropic coupled-field inclusion and inhomogeniety problems. Philos. Mag. A 77, 1341–1350.
Lutsko, J.F., 1988. Stress and elastic constants in anisotropic solids: Molecular dynamics techniques. J. Appl. Phys. 64, 1152–1154.
Maradudin, A.A., Montroll, E.W., Weiss, G.H., Ipatova, I.P., 1971. In: Ehrenreich, H., Turnbull, D., Seitz, F. (Eds.), Solid State Physics, Suppl. 3, second ed. Academic Press, New York.
McFarland, A.W., Colton, J.S., 2005. Role of material microstructure in plate stiffness with relevance to microcantilever sensors. J. Micromech. Microeng. 15, 1060–1067.
Metrikine, A.V., Askes, H., 2002a. One-dimensional dynamically consistent gradient elasticity models derived from a discrete microstructure: Part 1: generic formulation. Eur. J. Mech. A 21, 555–572.
Metrikine, A.V., Askes, H., 2002b. One-dimensional dynamically consistent gradient elasticity models derived from a discrete microstructure: Part 2: generic formulation. Eur. J. Mech. A 21, 555–588.
Meyers, M.T., Rickman, J.M., Delph, T.J., 2005. The calculation of elastic constants from displacement fluctuations. J. Appl. Phys. 98, 066106–066108.
Mi, C., Kouris, D., 2006. Nanoparticles under the influence of surface/interface elasticity. J. Mech. Mater. Struct. 1, 763.
Miller, R.E., Shenoy, V.B., 2000. Size-dependent elastic properties of nanosized structural elements. Nanotechnology 11, 139–147.
Mindlin, R.D., 1964. Micro-structure in linear elasticity. Arch. Rat. Mech. Anal. 16, 51–78.
Mindlin, R.D., 1965. Second gradient of strain and surface tension in linear elasticity. Int. J. Solids Struct. 1, 417–438.
Nikolov, S., Han, C.S., Rabbe, D., 2006. On the origin of size effects in small-strain elasticity. Int. J. Sol. Struct. doi: 10.1016/j.ijsolstr.2006.06.039.
Onck, P.R., 2003. Scale effects in cellular metals. MRS Bull. 28, 279–283.

Opie, A.H., Grindlay, J., 1972. Calculation of the coefficients describing the linear dependence of the stress tensor on the second order material gradients of the displacement gradients: rare gas solids. J. Phys. C: Solid State Phys. 5, 3289–3295.

Park, S.K., Gao, X.-L., 2006. Bernoulli–Euler beam model based on a modified couple stress theory. J. Micromech. Microeng. 16, 2355–2359.

Parrinello, M., Rahman, A., 1982. Strain fluctuations and elastic constants. J. Chem. Phys. 76, 2662–2666.

Portigal, D.L., Burnstein, E., 1968. Acoustical activity and other first-order spatial dispersion effects in crystals. Phys. Rev. 170, 673–678.

Pratt, L.R., 1987. Fluctuation method for calculation of elastic constants of solids. J. Chem. Phys. 87, 1245–1247.

Price, D.L., Rowe, J.M., Nicklow, R.M., 1971. Lattice dynamics of grey tin and indium antimonide. Phys. Rev. B 3, 1268–1279.

Ray, J.R., 1983. Molecular dynamics equations of motion for systems varying in shape and size. J. Chem. Phys. 79, 5128–5130.

Ray, J.R., Moody, M.C., Rahman, A., 1985. Molecular dynamics calculations of elastic constants for a crystalline system in equilibrium. Phys. Rev. B 32, 733–735.

Ray, J.R., Moody, M.C., Rahman, A., 1986. Calculation of elastic constants using isothermal molecular dynamics. Phys. Rev. B 33, 895–899.

Reid, A.C.E., Gooding, R.J., 1992. Inclusion problem in a two-dimensional nonlocal elastic solid. Phys. Rev. B 46, 6045–6049.

Ru, C.Q., Aifantis, E.C., 1993. A simple approach to solve boundary-value problems in gradient elasticity. Acta Mech. 101, 59–68.

Sharma, P., Dasgupta, A., 2002. Scale-dependent average of spherical and cylindrical inhomogenities in micropolar medium and overall properties. Phys. Rev. B 66, 224110-1–224110-10.

Sharma, P., Ganti, S., 2004. Size-dependent Eshelby's tensor for embedded nano-inclusion incorporating surface/interface energies. J. Appl. Mech. 71, 663–671.

Sharma, P., Ganti, S., Bhate, N., 2003. The effect of surfaces on the size-dependent elastic state of (nano) inhomogeneities. Appl. Phys. Lett. 82, 535–537.

Shibutani, Y., Vitek, V., Bassani, J.L., 1998. Non-local properties of inhomogeneous structures by linking approach of generalized continuum to atomistic model. Int. J. Mech. Sci. 40, 129–137.

Stafford, C.M., Harrison, C., Beers, K.L., Karim, A., Amis, E.J., Vanlandingham, M.R., Kim, H.C., Volksen, W., Miller, R.D., Simonyi, E.E., 2004. A buckling-based metrology for measuring the elastic moduli of polymeric thin films. Nat. Mater. 3, 545–550.

Steigmann, D.J., Ogden, R.W., 1999. Elastic surface–substrate interactions. Proc. R. Soc. A 455, 437–474.

Tersoff, J., 1988. Empirical interatomic potential for carbon, with applications to amorphous carbon. Phys. Rev. Lett. 61, 2879–2882.

Toupin, R.A., 1962. Elastic materials with couple-stresses. Arch. Rat. Mech. Anal. 11, 385–414.

Truesdell, C., Noll, W., 1992. The Non-Linear Field Theories of Mechanics. Springer, Berlin.

Vashishta, P., Kalia, R.K., Rino, J.P., 1990. Interaction potential for SiO_2: a molecular-dynamics study of structural correlations. Phys. Rev. B 41 (17), 12197–12209.

Warner, M., 2003. Isotropic-to-cholesteric transition in liquid crystal elastomers. Phys. Rev. B 67, 011701–011706.

Yang, J., Guo, S., 2005. On using strain gradient theories in the analysis of cracks. Int. J. Fract. 133, L19–L22.

Zein, N.E., 1984. Density functional calculations of elastic moduli and phonon spectra of crystals. Sov. Phys. Solid State 26 (10), 1825–1828.

Zhang, X., Sharma, P., 2005a. Inclusions and inhomogeneities in strain gradient elasticity with couple stresses and related problems. Int. J. Solids Struct. 42, 3833–3851.

Zhang, X., Sharma, P., 2005b. Size dependency of strain in arbitrary shaped, anisotropic embedded quantum dots due to nonlocal dispersive effects. Phys. Rev. B 72, 195345-1–195345-16.

Zhang, X., Kun, K., Sharma, P., Yakobson, B.I., 2006. An atomistic and non-classical continuum field theoretic perspective of elastic interactions between defects (force dipoles) of various symmetries and application to graphene. J. Mech. Phys. Solids 54, 2304–2329.

Zhang, X., Sharma, P., Johnson, H.T., 2007. Quantum confinement induced strain in quantum dots. Phys. Rev. B, accepted for publication.

Zhou, Z., Joos, B., 2002. Fluctuation formula for the elastic constants of an arbitrary system. Phys. Rev. B 66, 054101–054107.